Mapping the GDF15 Arm of the Integrated Stress Response in Human Cells and Tissues

Janell L.M. Smith[1], Kamaryn Tanner[2], Jack Devine[1], Anna S. Monzel[1],

Taivan Batjargal[3], Maxwell Z. Wilson[3], Alan A. Cohen[2,4], Martin Picard[1,2,5,6]

[1] Department of Psychiatry, Division of Behavioral Medicine, Columbia University Irving Medical Center, New York, NY 10032, United States

[2] Robert N Butler Columbia Aging Center, Mailman School of Public Health, New York, NY 10032, United States

[3] Biomolecular Science and Engineering Program, University of California Santa Barbara, Santa Barbara, CA, USA

[4] Department of Environmental Health Sciences, Mailman School of Public Health, New York, NY 10032, United States

[5] Department of Neurology, H. Houston Merritt Center for Neurological and Mitochondrial Disorders, Columbia University Irving Medical Center, New York, New York 10032, United States

[6] New York State Psychiatric Institute, New York, NY 10032, United States

* Correspondence: martin.picard@columbia.edu

Abstract

Mitochondrial stress activates the integrated stress response (ISR) and triggers cell–cell communication through the secretion of the metabokine growth differentiation factor 15 (GDF15). However, the gene network underlying the ISR remains poorly defined, particularly across metabolically diverse cellular states and tissues. Using RNAseq data from fibroblasts subjected to eleven metabolic perturbations, including genetic and pharmacological mitochondrial OxPhos defects, we showed that the ISR has multiple arms and developed an ISR^{GDF15} index quantifying the GDF15 arm of ISR activation in human cells. The ISR^{GDF15} index was validated using optogenetic activation of the ISR protein kinase R (PKR) in a stable cell line, demonstrating its rapid kinetics preceding to *GDF15* gene expression. We then deployed the ISR^{GDF15} index across 44 postmortem human tissues, reporting that the ISR^{GDF15} was upregulated in the heart of individuals who died of an acute cause in the emergency room, whereas it was preferentially upregulated in the brain of individuals who died as inpatients after protracted hospital stays. ISR^{GDF15} was also moderately, positively correlated with age across all tissues. These data highlight multiple distinct ISR pathways and clarify which genes are related to the GDF15 arm of the ISR, yielding an ISR^{GDF15} index that can be used to investigate tissue-specific and age-related ISR activation in both in vitro cultures and human tissues. Ultimately, we expand our knowledge of the GDF15 arm of the ISR in humans, show its inducibility by the ISR kinase PKR, and demonstrate its applicability to detect ISR activation in specific human tissues.

Keywords: Integrated stress response, energetic stress, GDF15, metabolism, OxPhos, cause of death, aging, brain

Main Text

Cells sense reductive stress via the integrated stress response (ISR)[1]. Among many targets, the ISR activates the gene *GDF15*, which encodes a secreted cytokine/metabokine known to be elevated with aging[2] and in several chronic diseases[3,4]. This elevation is particularly strong in primary mitochondrial diseases caused by defects in the oxidative phosphorylation (OxPhos) system[5,6]. However, the ISR is pleiotropic and triggers multiple cellular processes[7]. As a result, there is no consensus on the gene network that constitutes the ISR in human cells, or whether the same set of genes operate in metabolically diverse organs or tissues. Here, we seek to understand the dimensionality of the ISR, with a particular focus on the pathway or "arm" leading to GDF15 signaling, given its status as an ISR biomarker[8] and its role in mediating the ISR[9].

To identify ISR-related genes linked to inter-cellular GDF15 signaling, we queried multiple ISR gene lists (119 genes in total)[10-12] (**Figure 1A**), and examined their co-expression in a cellular-lifespan-system dataset generated in fibroblasts[13]. Sensitivity analyses were performed on each gene list separately, as well as a random selection of 119 selected genes out of all mapped genes in the RNAseq dataset. This process demonstrated the superiority of including all 119 genes from the combined lists, plus *GDF15*, in the fibroblast dataset, over using the individual ISR gene lists, equally loaded genes of the 119 combined genes, or 119 randomly chosen genes (**Extended Data Figure 1**).

We used a longitudinal transcriptomic dataset including 339 fibroblast samples collected from either healthy donors or mitochondrial-disease donors with mutations in the OxPhos complex IV assembly-factor gene *SURF1* (**Figure 1B**). To create a vast spectrum of bioenergetic conditions, each cell line was exposed to up to 11 metabolic perturbations including an inhibitor of the OxPhos system, oligomycin (Oligo), glucocorticoid agonist dexamethasone (DEX), mitochondrial-nutrient-uptake inhibitors (mitoNUITs), glucose deprivation plus β-hydroxybutyrate (BHB), low oxygen (3%), and contact inhibition[13]. OxPhos defects are potent triggers of the ISR in other datasets[1] and in this dataset[14], making this model and the variety of conditions tested an ideal testbed to examine gene expression signatures of the GDF15 arm, and other dimensions of the ISR, in human cells (**Figure 1C**).

To computationally isolate co-regulated ISR genes, we queried bulk gene expression RNAseq data using *GDF15* as a bait; we included *GDF15* alongside the 119 ISR genes from the three ISR gene lists and performed dimensionality-reduction analyses (the 120 genes can be found in **Extended Data Table 1)**. This allowed us to explore gene expression patterns within our samples, with a focus on patterns most strongly associated with *GDF15*. Using principal component analysis (PCA) to explore this gene-expression landscape across all treatments simultaneously (**Figure 1D**), we identified a major axis of genes co-regulated with *GDF15* (principal component 2, explains 15.5% of variance). **Extended Data Figure 2A** shows the loadings for each gene on each of the first two principal components.

Next, we used factor analysis to more quantitatively isolate the transcriptional signature of this *GDF15*-related ISR axis. This approach converged on an optimal solution containing 12

factors (i.e., sets of loadings or "weights" applied to each of the 119 genes plus *GDF15* for a total of 120 genes), which collectively account for a maximal portion (73.1%) of the shared variance within this dataset (**Figure 1E**). The relationships between the principal components and each factor are quantified in **Extended Data Figure 5A,** with specific correlation plots depicted in **Extended Data Figure 5B-C**. Factor 1—our index hereafter referred to as the ISR^{GDF15} score—explained 12.9% of the variance, and was more strongly correlated with *GDF15* expression (Spearman's rank correlation coefficient (ρ) = 0.87, $p<1x10^{-15}$) than any other factor, establishing construct validity for the calculated ISR^{GDF15} score (**Figure 1F**). The 11 remaining factors and their gene loadings, which are not explored in this work but available to readers in **Extended Data Table 2**, may represent additional pathways indicative of other ISR dimensions.

To understand the biology underlying the ISR^{GDF15} index, we compared the genes most strongly associated (positively or negatively) with *GDF15*. The genes contributing most strongly to the ISR^{GDF15} index were positively enriched for regulation of endoplasmic reticulum–unfolded protein response [top $10_{positive}$: *DDIT3*, *PPP1R15A*, *ERN1*, *GADD45A*, *CBX4*, *BBC3*, *SLC3A2*, *SIAH2*, *CEBPB*, *TRIB3*]. In contrast, negatively weighted genes for the ISR^{GDF15} index were enriched for the regulation of translation and translation initiation [top $10_{negative}$: *PPP1CA*, *APAF1*, *SLC35A4*, *FOS*, *IMPACT*, *NAIP*, *BIRC5*, *EIF2B1*, *NARS1*, *GCN2*] (see **Extended Data Table 3** annotations and known functions of each gene), a well-described consequence of ISR activation in most cell types. These results are also consistent with the notion that cellular processes operate under energy constraints: that is, while the activation of some energy-dependent processes are upregulated, other processes must be downregulated[15,16]. As such, cells activating the GDF15-signaling ISR arm may generally downregulate protein synthesis, as previously observed[17], despite known increases in specific proteins, including GDF15[14,18].

Functionally, ISR^{GDF15} was most significantly induced in oligomycin-treated cells (large effect size, g = 2.13, p< 0.001) and in SURF1-mutant cells (g = 1.91, p<0.001, **Figure 1G**) relative to untreated control cells, as expected. The conditions of no glucose with β-hydroxybutyrate (g = 1.33, p<0.001) and the glycolysis inhibitor 2-deoxyglucose (g = 0.97, p<0.05) also resulted in a higher ISR^{GDF15}, which is consistent with glucose deprivation being a known ISR activator[19]. The higher ISR^{GDF15} observed in the contact-inhibition condition (g = 1.23, p<0.001) was surprising at first, as it was expected to be more physiologically similar to what cells experience in vivo (i.e., a more physiological skin cell culture). However, the culture protocol used in this condition called for only one media change per week (matching the passaging of the non-contact-inhibited cells). This protocol led to a higher density of cells throughout the week, which, in turn, may have depleted nutrients at a faster rate. Thus, the ISR was likely activated in the contact-inhibition group as a result of nutrient starvation.

To our initial surprise, the low oxygen level (3%, not anoxia) treatment was not an activator of the ISR, as would be logically expected of a hypoxic treatment. However, upon reviewing the literature, we noted that the experimental conditions previously considered hypoxic treatments for these fibroblast cells was, in fact, likely a physiological oxygenation level [20]. In vivo skin has oxygenation levels between 1.1-4.6%[20], and thus is likely to be a better control than our control group, which is cultured at 21% oxygen. Together, these data

demonstrate the existence of a relatively small subset of positively and negatively inducible *GDF15*-related ISR genes induced by mitochondrial OxPhos perturbations.

To validate the ISR^{GDF15} index, we then tested how targeted and time-resolved ISR activation influenced GDF15 itself, and the ISR^{GDF15} index. To achieve this, we used data from a light-activatable protein kinase R (PKR) kinase in the H4 cancer line (**Figure 2A**)[21]. This optogenetic model triggers robust activation of the ISR (marked by p-eIF2a, ATF4, and CHOP induction) without other confounds including the simultaneous activation of other pathways, such as damage response pathways, for example.

The light sensitive–PKR H4 cells were stimulated with light for up to 12 hours, and cells harvested at eight timepoints for bulk RNAseq (**Figure 2B**). We deployed the ISR^{GDF15} index to the RNAseq data, quantifying its expression at each timepoint (See **Figure 2C)**. The ISR^{GDF15} score increased by 1 hour and peaked at 6-8 hours, followed by a plateau over the remaining hours of light stimulation. The trajectories of induction for other factor scores are shown in **Extended Data Figure 6A**.

Comparatively, PKR activation did not induce *GDF15* expression over the first 4 hours. However, between hours 4 and 6 we observed a ~5-fold increase in GDF15 mRNA at 6 hours (**Figure 2C**). Together, these findings support the accuracy and sensitivity of the ISR^{GDF15} index to PKR-mediated ISR activation, even in the absence of changes in *GDF15* expression from 0 to 4 hours. This suggests that the ISR^{GDF15} index captures ISR biology more broadly and sensitively than *GDF15* alone.

To examine the extent to which the ISR^{GDF15} index it is conserved in human tissues, we used the Genome-Tissue Expression (GTEx) project, which includes RNAseq data on up to 17 different organs from ~1,000 donors[22] (**Figure 3A left**). We first asked whether the ISR^{GDF15} score was correlated with its bait *GDF15* gene, when applied to individual human organs and tissues. If the internal correlation structure and loadings of the genes composing the ISR^{GDF15} index were similar across datasets, we expected positive correlations between the index and the gene *GDF15*. Focusing on tissues with a sample size >20, we observed significant positive correlations between the ISR^{GDF15} and *GDF15* in 43 out of 44 (97.7%) human tissues (ρ = 0.41-0.82, all p's <0.05 corrected for multiple testing, **Figure 3B**). These findings suggest that the genetic architecture of the *GDF15*-related arm of the ISR is at least partially conserved between fibroblasts in vitro and human tissues in vivo.

Given the well-known upregulation of GDF15 with age[2], but not necessarily of the ISR per se, we examined the association of ISR^{GDF15} score with age in GTEx (range 20-70, average 53 years). The correlations were positive as expected in all human tissues, and 33 of 44 tissues were significant (average ρ = 0.23, p<0.001, **Figure 3D**). Seeking a generalizable test to examine how different gene expression-based indices perform across fibroblasts and human tissues, we average expression across all tissues and individuals of different health status included in the dataset. GDF15 alone also was correlated with age, and in some tissues more strongly so than the ISR^{GDF15} score (**Figure 3D**).

To pressure test this analysis further, we confirmed that senescence-associated genes (averaged tissue expressions of *CDKN1A*, *CDKN2A*, *CCND2*) were upregulated, whereas proliferative or replication-related genes (averaged tissue expressions of *TOP2A*, *RRM2*, *MKI67*) were downregulated with advancing age, validating the use of cellular lifespan system[13] to probe time- or age-related changes. Other single ISR genes *ATF4* and *ATF5* were unrelated to age, whereas *CHOP* was mildly related to age (ρ = 0.13, p<0.001) with about half the effect size of *GDF15*. In sum, ISR^{GDF15} was positively associated with age (ρ = 0.19, p<0.001), indicating that the *GDF15*-related arm of the ISR is upregulated with age, and more strongly than individual genes classically referenced alone (or in conjunction with others) to denote activation of the ISR (**Figure 3D**).

We then systematically examined the other 11 potential arms of the ISR isolated by factor analysis, ranked from negative to positive age-related effect sizes across all GTEx tissues (**Figure 3D**). Four other ISR arms were significantly negatively associated with age (Factors 12, 6, 2, 4), and one was positively associated with age (Factor 11). Applying the same analysis to aging human fibroblasts similarly showed both *GDF15* alone (ρ = 0.51, p<0.001) and the ISR^{GDF15} score (ρ = 0.61, p<0.001) were positively associated with age, though these effect sizes were smaller than the senescence associated markers (ρ = 0.77, p<0.001), as expected.

A direct comparison of effect sizes across each gene, the ISR^{GDF15} *score*, and the 11 factors revealed a moderate correlation between the in vivo and in vitro datasets (ρ = 0.69, p<0.01, **Extended Data Figure 7A left**). The correlation was stronger without the 11 non-ISR^{GDF15} factors (ρ = 0.93, p<0.01, **Extended Data Figure 7A right**). Given the coherence between the two systems (in vivo and in vitro), this finding supports the notion that the ISR^{GDF15} signaling arm has an age-related association similar to that of *GDF15* in both strength and direction. In other words, the ISR^{GDF15} index accounts for most of the age-related signal of the ISR. The other factors may be important processes, but their age associations are considerably weaker than the identified ISR^{GDF15} arm.

In the GTEx dataset, some donors died suddenly in the intensive care unit (76.4% of a cardiac arrest or related cause), while other individuals were hospital inpatients that endured more protracted death processes (involving coma, or other conditions). To test whether ISR activation was associated with organ-specific cause of death, we calculated the ISR^{GDF15} score for each tissue for each place of death: emergency room (ER) and hospital inpatient (HI). We focused on these groups for two reasons: i) each group included a sufficient number of samples to allow robust comparisons of ISR activation; and ii) acute ER deaths are more likely to have been associated with acute cardiocirculatory death within hours, while HI deaths are more likely to have endured metabolic disturbances and an protracted agonal period that tends to affect brain function (e.g., coma). Because the ISR is activated in a time-dependent manner[7], we hypothesized that longer hospital stays and pathology in HI would produce higher ISR^{GDF15} activation compared to ER donors, who on average had less time to activate the ISR before death.

The expected ISR activation pattern was only observed in a specific subset of tissues: brain, salivary gland, skeletal muscle, skin, tibial nerve and artery, and subcutaneous adipose

tissue (no digestive tissues). We also found that donors from the ER had significantly higher ISR^{GDF15} scores in a different subset of tissues: whole blood, mammary breast, prostate, thyroid, esophageal, lung, transverse colon, stomach and the atrial appendage, left ventricle, aorta, and coronary artery of the heart; not in CNS tissues (**Figure 4C)**.

To investigate this unexpected pattern, we drew upon previous research by Mick et al., which demonstrated that the same stressor triggered differential ISR activation between myoblasts (actively proliferating) compared to myotubes (non-proliferative)[1]. To explore whether proliferation status could contribute to the differential ISR activation across human tissues, we calculated the proliferation score of each tissue [23] (see methods for details) and split the tissues into two groups: proliferative vs non-proliferative, using the median proliferation score. We then compared the ISR^{GDF15} scores between the two groups based on their proliferation status. Proliferative tissues exhibited significantly higher ISR activation scores than the non-proliferative tissues (**Extended Data Figure 8A**). This was validated by the significant correlation between ISR activation scores and proliferation scores across tissues (ρ = 0.78, p<0.001, **Figure 4D**). Finally, we categorized the tissues according to whether the donors had significantly higher ISR^{GDF15} scores based on deathplace (either HI to ER or ER to HI), and found that the two groups had different proliferative indexes (g = 1.17, p<0.01, **Figure 4E**). The tissues with higher ISR^{GDF15} in the ER group were more proliferative than those that were higher in the HI group. Ultimately, these analyses support the notion that proliferation status contributes to differential ISR activation in a tissue-dependent manner, and help explain the distribution of ISR activation observed across tissues according to place of death seen in **Figure 4C.**

Interestingly, in these post-mortem tissues, ISR^{GDF15} was more sensitive than *GDF15* expression to sudden death vs chronic illness (or vice versa), as reflected by 81.6% of tissues showing significantly different ISR^{GDF15} scores under these two scenarios compared to only 52.6% of tissues showing a significant difference in *GDF15* expression under the same scenarios (Chi square = 5.96, p = 0.015, **Figure 4C**). This was exemplified in the frontal cortex of the brain, which displayed a large effect size (g = 0.91) for ISR^{GDF15} when comparing sudden death to chronic illness, but only a moderate effect size for *GDF15* (g = 0.57, **Figure 4B**). These results are meaningful, particularly in the context of a robust correlation between ISR^{GDF15} and *GDF15* expression in this tissue (ρ = 0.74, **Figure 4A**). This supports the use of the ISR^{GDF15} score rather than *GDF15* alone as an indicator of ISR activation.

Discussion

Together, this work challenges the monolithic understanding of the ISR in humans, showing instead that the ISR—as defined by popular gene lists[10-12]—contains distinct sub-responses or sub-pathways. In particular, our results highlight potential tissue-specificity in ISR activation with disease and conditions leading up to death (see **Figure 4C-E**). These findings call for the consideration of tissue-specific regulatory mechanisms or downstream effects that have yet to be defined. We also identify a conserved set of *GDF15*-related canonical ISR genes upregulated by experimental mitochondrial perturbations, as well as other groups of genes (factors 2-12) that reflect the multidimensional nature of the ISR. The identified ISR^{GDF15} index

and *GDF15* expression were co-regulated across most human tissue, and some aspects of the ISR genetic architecture (*ISR*^{GDF15} in particular) were found to be conserved across three distinct datasets, increasing our confidence in the robustness of these findings. Finally, this work illustrates that *ISR*^{GDF15} is activated in a time-dependent manner that precedes *GDF15* expression, making it an indicator of early (pre-GDF15 induction) ISR detection.

The limitations of this study include i) the use of linear statistical methods, while genes likely interact in non-linear ways[24], ii) analyses from post-mortem human tissues, where the post-mortem period could alter gene expression profiles, at least in the brain[25], iii) the optogenetic experiments were only performed with a single ISR kinase, which, while sufficient to robustly induce the ISR[21] may not paint the full picture of ISR biology. We also note that the genes from the literature-based consensus lists could be missing other important genes. Further work to demonstrate the activation or inactivation of the index could be performed with the use of ISR inhibitors such as ISRIB, which would provide a negative control that was not available in these experiments. This would be especially useful for opto-PKR, given the relatively high baseline expression of *GDF15* observed here, which is consistent with high GDF15 expression in several cancer cell lines (see Human Protein Atlas[26]).

Overall, we present a general approach to develop multi-gene indices, and the *ISR*^{GDF15} index in particular provide a foundation for future research aiming to dissect the multifaceted biology of the human ISR in relation to health, disease, and aging.

Methods

ISR Gene List Compilation

Gene lists for the ISR were gathered by inputting the phrase “integrated stress response” into the search bars of the main websites for three sources: GO Consortium, The Jackson Laboratory, and Any Genes[10-12]. The genes from each lists were merged to make one combined ISR gene list. Some gene names were altered to fit the nomenclature of the specific transcriptomic dataset being used, as different gene aliases were used in each dataset for some genes (i.e., NARS1/NARS, WARS1/WARS, Igtp/IRGM). The genes found in each gene list are reported in **Extended Data Table 1**. Information about the top 10 positively and negatively associated genes in the *ISR*^{GDF15} index was found by searching each gene in URL: https://www.genecards.org/.

Fibroblast Lifespan Study

The lifespan study is explained in full detail in Sturm et al[13]. RNAseq data was downloaded from the shiny app URL: https://columbia-picard.shinyapps.io/shinyapp-Lifespan_Study/. Fibroblast transcriptomic data was previously normalized via DEseq2, v1.30.1, and was log2 transformed. A total of 339 samples (excluding control line technical replicate data) was used for further analysis. Five healthy control lines and three patient-derived SURF1 mutant lines were cultured, with or without various metabolic treatments, as described in Sturm et al.[13,14].

PCA

R version 4.4.1 with R studio was used to perform PCA (and all subsequent statistical analyses). The 'prcomp' function was used to generate PCA, (*stats* package v4.4.1) using 339 fibroblast samples and the master list of ISR genes plus *GDF15*. Principal component biplots of components beyond PC1 vs PC2 are plotted in **Extended Data Figure 3**, as well as their correlations against fibroblast days in culture in **Extended Data Figure 2B-C**.

Factor Analysis

The same fibroblast dataset of 339 samples and 120 genes was used in the factor analysis. The 'factanal' function (*stats* package) was used, with a varimax rotation. The scree method[27] was used to determine the number of factors, as no predetermined number was hypothesized given that the number of causes and outputs of the ISR have yet to be determined. Of the 119 ISR genes, the ISR^{GDF15} index included 77 positive and 42 negative gene loadings, reflecting ISR genes positively and negatively related to *GDF15* (see **Extended Data Table 4** for individual gene loadings). Individual genes, such as *GDF15*, were centered and scaled by using the scale() function in R before comparing against the ISR^{GDF15} score or age. A biplot of ISR^{GDF15} (Factor 1) vs Factor 2, as well as all factor scores compared to age are depicted in **Extended Data Figure 4**.

Opto-PKR ISR Score

Raw FPKM values were normalized to TPM from Batjargal et al. and was log2 transformed. Then, the values were centered and scaled to the initial fibroblast dataset, and finally the ISR^{GDF15} index was applied, as depicted in the bottom half of **Figure 2B.**

GTEx

RNA sequencing data was downloaded as gene expression read counts from GTEx Analysis V8. RNA integrity number (RIN) values of less than 6 were filtered out of the data. Trimmed Mean of M-values (TMM) values were calculated using DGE method (BiocGenerics package, version 0.50.0). To convert the human TMM values to the ISR^{GDF15} score, human data were scaled to the initial fibroblast dataset, as depicted in **Figure 2B** (by subtracting the human TMM values by fibroblast means and dividing by the fibroblast standard deviation), and applied to the correlation matrix of the initial fibroblast data to the human data. Tissue samples of less than 20 were excluded from the analysis, leaving the kidney cortex with the minimum number of tissue samples of 86. Four tissues were excluded from the application of the ISR^{GDF15} index due to missing one or more genes from the ISR list: bladder, brain cerebellar hemisphere, brain cerebellum, and adrenal gland. A total of 44 tissues were included in the analyses. Three genes required changing aliases to match the fibroblast genes: *DELE1* was changed to *KIAA0141*, *WARS1* was changed to *WARS*, and *NARS1* was changed to *NARS*. When comparing either the ISR^{GDF15} score of ER vs HI or *GDF15* of ER vs HI, tissues with less than 20 samples per group (ER or HI), were filtered out. Six tissues were filtered out: kidney cortex, pancreas, small intestines of the ileum, spleen, uterus, and vagina for having less than 20 samples in the ER

group. For distinguishing cardiac-related deaths within the HI or ER groups, we included the following terms as cardiac-related under the cause of death columns either DTHCOD or DTHFUCOD: “cardiac”, “acute mi”, “myocardial”, “myocardiac”, “arrest”, “cardio”, “bradycardia”, “heart”, “aortic dissection”, “probable mi”, and “chf”. Causes of death that did not include any of those terms were deemed non-cardiac. The HI group was composed of 25.2% cardiac-related deaths. Various tissues in the GTEx dataset were noted in the pathology notes column to contain other tissues (often fat) these samples were not filtered out.

Tissue Groups

As described in Devine et al.[23], tissues were split into the following groups: liver into Anabolic; all brain tissues into central nervous system (CNS); skeletal muscle, heart atrial appendage and heart left ventricle into Contractile; colon tissues, esophageal tissues, and stomach into Digestive; testis, ovary, and prostate into Reproductive; salivary gland, adipose subcutaneous and visceral omentum, thyroid, and pituitary into Secretory; skin lower leg and suprapubic, artery tibial, breast mammary, whole blood, artery coronary, lung, and artery aorta into Other.

Senescence and Proliferation Index Scores

Genes for senescence (*CDKN1A*, *CDKN2A*, *CCND2*)[28] or proliferation (*TOP2*, *RRM2*, *MKI67*)[23] were selected to create either a tissue senescence score or proliferation score, by averaging the three senescent or proliferative genes respectively. Selection criteria for the proliferation index genes are explained in the methods of Devine et al.[23]. When splitting the tissues into two groups, proliferative vs non-proliferative, the median score of 0.63 was used.

Statistics

All correlations performed were Spearman’s rank correlations. When comparing group differences of two groups, Wilcoxon rank-sum tests were used. When noted, Bonferroni correction for multiple comparisons was used, with a p-value threshold of 0.05. Otherwise, we used the Benjamini-Hochberg (BH) method, a less stringent form of multiple testing corrections, for more exploratory questions. Effect sizes were determined via Hedge’s g, an unbiased analog of Cohen’s d[29]. Hedge’s g was calculated via the R function ‘cohen.d’ from the package *effsize*, with the Hedge’s g correction applied. When comparing multiple independent treatment groups simultaneously, Prism version 10.2.3 (347) was used to perform a Kruskal-Wallis test followed by Dunn’s test for multiple comparisons. Wilcoxon signed-rank test was performed using Prism, when testing if a group significantly differed from 0.

Acknowledgements

Some figure elements were generated with Biorender.com. We are grateful to the GTEx consortium and to Gabriel Sturm for creating the valuable Cellular Lifespan Study data resources that made this work possible.

Author contributions

J.L.M.S and M.P. conceived the project. J.L.M.S. performed the analyses with K.T. J.L.M.S. generated the figures. J.L.M.S., M.P., A.A.C., K.T., A.S.M., and J.D. interpreted the data. T.B. and M.Z.W provided data for the optogenetic ISR activation. J.L.M.S., and M.P. drafted the manuscript with A.A.C. All authors reviewed and edited the final manuscript.

Funding

This work was supported by NIH grants R35GM119793, R01AG066828, R01AG086764, the Wharton Fund, and Baszucki Group to M.P.

Data and code availability

GTEx v8 RNAseq data is available for download at https://gtexportal.org/home/downloads/adult-gtex/bulk_tissue_expression.Cellular. The Lifespan Study fibroblast dataset can be downloaded at https://columbia-picard.shinyapps.io/shinyapp-Lifespan_Study/. R code for the analyses will be made available at www.github.com/mitopsychobio .

Competing Interests

The authors declare no competing interests in regard to this work.

Extended Data Material

This article contains 8 Extended Data Figures and 4 Extended Data Tables.

References

1 Mick, E. *et al.* Distinct mitochondrial defects trigger the integrated stress response depending on the metabolic state of the cell. *Elife* **9** (2020). https://doi.org:10.7554/eLife.49178

2 Conte, M. *et al.* GDF15, an emerging key player in human aging. *Ageing Res Rev* **75**, 101569 (2022). https://doi.org:10.1016/j.arr.2022.101569

3 Deng, Y. T. *et al.* Atlas of the plasma proteome in health and disease in 53,026 adults. *Cell* **188**, 253-271 e257 (2025). https://doi.org:10.1016/j.cell.2024.10.045

4 You, J. *et al.* Plasma proteomic profiles predict individual future health risk. *Nat Commun* **14**, 7817 (2023). https://doi.org:10.1038/s41467-023-43575-7

5 Sharma, R. *et al.* Circulating markers of NADH-reductive stress correlate with mitochondrial disease severity. *J Clin Invest* **131** (2021). https://doi.org:10.1172/JCI136055

6 Hubens, W. H. G. *et al.* Blood biomarkers for assessment of mitochondrial dysfunction: An expert review. *Mitochondrion* **62**, 187-204 (2022). https://doi.org:10.1016/j.mito.2021.10.008

7 Labbe, K. *et al.* Specific activation of the integrated stress response uncovers regulation of central carbon metabolism and lipid droplet biogenesis. *Nat Commun* **15**, 8301 (2024). https://doi.org:10.1038/s41467-024-52538-5

8 Asundi, J. *et al.* GDF15 is a dynamic biomarker of the integrated stress response in the central nervous system. *CNS Neurosci Ther* **30**, e14600 (2024). https://doi.org:10.1111/cns.14600

9 Kim, K. H. & Lee, M. S. GDF15 as a central mediator for integrated stress response and a promising therapeutic molecule for metabolic disorders and NASH. *Biochim Biophys Acta Gen Subj* **1865**, 129834 (2021). https://doi.org:10.1016/j.bbagen.2020.129834

10 AnyGenes. UNDERSTANDING THE INTEGRATED STRESS RESPONSE (ISR). (2025).

11 Laboratory, T. J. Gene Ontology Annotations. (2024).

12 Consortium, G. O. *"Gene Ontology Resource."*, <https://geneontology.org/> (2025).

13 Sturm, G. *et al.* A multi-omics longitudinal aging dataset in primary human fibroblasts with mitochondrial perturbations. *Sci Data* **9**, 751 (2022). https://doi.org:10.1038/s41597-022-01852-y

14 Sturm, G. *et al.* OxPhos defects cause hypermetabolism and reduce lifespan in cells and in patients with mitochondrial diseases. *Commun Biol* **6**, 22 (2023). https://doi.org:10.1038/s42003-022-04303-x

15 Yang, X. *et al.* Physical bioenergetics: Energy fluxes, budgets, and constraints in cells. *Proc Natl Acad Sci U S A* **118** (2021). https://doi.org:10.1073/pnas.2026786118

16 Wieser, W. & Krumschnabel, G. Hierarchies of ATP-consuming processes: direct compared with indirect measurements, and comparative aspects. *Biochem J* **355**, 389-395 (2001). https://doi.org:10.1042/0264-6021:3550389

17 Kaspar, S. *et al.* Adaptation to mitochondrial stress requires CHOP-directed tuning of ISR. *Sci Adv* **7** (2021). https://doi.org:10.1126/sciadv.abf0971

18 Young, S. K. & Wek, R. C. Upstream Open Reading Frames Differentially Regulate Gene-specific Translation in the Integrated Stress Response. *J Biol Chem* **291**, 16927-16935 (2016). https://doi.org:10.1074/jbc.R116.733899

19 Pakos-Zebrucka, K. *et al.* The integrated stress response. *EMBO Rep* **17**, 1374-1395 (2016). https://doi.org:10.15252/embr.201642195

20 Carreau, A., El Hafny-Rahbi, B., Matejuk, A., Grillon, C. & Kieda, C. Why is the partial oxygen pressure of human tissues a crucial parameter? Small molecules and hypoxia. *J Cell Mol Med* **15**, 1239-1253 (2011). https://doi.org:10.1111/j.1582-4934.2011.01258.x

21 Batjargal, T. *et al.* Optogenetic control of the integrated stress response reveals proportional encoding and the stress memory landscape. *Cell Syst* **14**, 551-562 e555 (2023). https://doi.org:10.1016/j.cels.2023.06.001

22 Consortium, G. T. The Genotype-Tissue Expression (GTEx) project. *Nat Genet* **45**, 580-585 (2013). https://doi.org:10.1038/ng.2653

23 Devine, J. *et al.* Brain-body mitochondrial distribution patterns lack coherence and point to tissue-specific and individualized regulatory mechanisms. *bioRxiv* (2024). https://doi.org:10.1101/2024.09.20.614152

24 Kontio, J. A. J., Rinta-Aho, M. J. & Sillanpaa, M. J. Estimating Linear and Nonlinear Gene Coexpression Networks by Semiparametric Neighborhood Selection. *Genetics* **215**, 597-607 (2020). https://doi.org:10.1534/genetics.120.303186

25 Liharska, L. E. *et al.* A study of gene expression in the living human brain. *medRxiv* (2023). https://doi.org:10.1101/2023.04.21.23288916

26 Atlas, T. H. P. <https://www.proteinatlas.org/ENSG00000130513-GDF15/cell+line> (2024).

27 Cattell, R. B. The Scree Test For The Number Of Factors. *Multivariate Behav Res* **1**, 245-276 (1966). https://doi.org:10.1207/s15327906mbr0102_10

28 Bertolo, A., Baur, M., Guerrero, J., Potzel, T. & Stoyanov, J. Autofluorescence is a Reliable in vitro Marker of Cellular Senescence in Human Mesenchymal Stromal Cells. *Sci Rep* **9**, 2074 (2019). https://doi.org:10.1038/s41598-019-38546-2

29 Hedges, L. V. & Olkin, I. *Statistical methods for meta-analysis*. (Academic Press, 1985).

Figure legends

Figure 1. Development of an ISR index using primary human fibroblasts. (**A**) ISR related genes from three reference ISR pathway lists revealing minimal overlap. We use all 119 genes plus *GDF15* (n=120) to compile an unbiased ISR gene list. (**B**) Bulk RNA seq data in primary human fibroblasts from three healthy donors and three individuals with mitochondrial disease (SURF1 gene mutations) were cultured across their replicative lifespans (up to 260 days) and treated with pharmacological and metabolic perturbations, including the OxPhos inhibitor oligomycin (1nM). (**C**) Overview of the analytical strategy to generate an ISR index using *GDF15* as a bait. (**D**) Principal component analysis (PCA) of data from the lifespan study depicted in panel B including 339 samples 120 genes. The red arrow denotes the loading vector of *GDF15*; all other genes shown in **Extended Data Figure 2**. (**E**) Factor analysis revealed one factor where *GDF15* had the strongest positive loading (Factor 1, *left*), yielding weights that reflect the co-regulation of all other genes with *GDF15* (*right*). (**F**) Correlation of Factor 1 with standardized *GDF15* expression. (**G**) Boxplots of ISR^{GDF15} scores for each condition, sorted by ascending median score. P-values from Kruskal-Wallis test and Dunn's test for multiple comparisons. *Oligo,* Oligomycin; DEX = dexamethasone, mitoNUITs = mitochondrial nutrient uptake inhibitors, 2DG = 2-Deoxy-D-glucose, BHB = β-hydroxybutyrate, contact inhib = contact inhibition.

Figure 2. Validation of the ISR^{GDF15} index with time-resolved ISR activation. (**A**) Optogenetic ISR activation strategy targeting an engineered light-sensitive PKR, an ISR kinase, which phosphorylates eIF2alpha to activate the ISR, as per Batjargal et al. (**B**) Experimental and data processing scheme to compute the ISR^{GDF15} scores across 8 timepoints spanning 12 hours of continuous PKR activation in H4 cells. (**C**) ISR^{GDF15} score and *GDF15* RNA transcript levels for the H4 cells under increasing hours of ISR stimulation.

Figure 3. ISR^{GDF15} index applied to human GTEx dataset correlated with age at death. (**A**) Schematic of human GTEx dataset containing a variety of human organ samples, and applying the fibroblast generated index to the human transcriptomic data to get the human ISR^{GDF15} scores for each tissue. (**B**) ISR^{GDF15} correlations with *GDF15* across all the tissue samples expressing all 120 genes in the ISR^{GDF15} index (Spearman's ρ, +/- 95% confidence intervals, Bonferroni corrected for multiple comparisons). (**C**) Spearman's rank correlations of each tissue's ISR^{GDF15} score compared to donor age (red points denoting a Bonferroni corrected $p<0.05$). (**D**) Average Spearman's correlations (+/- SEM) across all 44 tissues comparing the

donor age with the chosen gene(s) or *ISR*^{GDF15} score or factor scores (left) and fibroblasts' age correlated with the chosen genes or *ISR*^{GDF15} score or factor score (+/- 95% confidence interval) (right). *ISR*^{GDF15} average tissue correlation denoted with a red triangle. Wilcoxon signed-rank test used compared against 0.

Figure 4. *ISR*^{GDF15} index applied to human GTEx dataset. (**A**) Select tissue correlations of *ISR*^{GDF15} and *GDF15* expression, Bonferroni corrected. (**B**) *ISR*^{GDF15} or *GDF15* expression for each place of death, in brain frontal cortex or heart left ventricle; significance determined via Wilcoxon rank-sum test. (**C**) Hedge's g effect sizes comparing each tissue's *ISR*^{GDF15} activation score for each place of death, or *GDF15* expression comparing each place of death—Hedge's g values of hospital inpatient scores being greater than ER seen on the right, ER greater than hospital inpatient towards the left. Circles denote *ISR*^{GDF15} score, squares *GDF15* expression, red as significant, gray non-significant, with BH correction for multiple comparisons. The grey brain and heart indicate the *ISR*^{GDF15} score and *GDF15* expression of the brain frontal cortex and the heart left ventricle comparisons from **B**. See methods for specific tissues within each tissue grouping. Wilcoxon rank-sum test was used to compare either the *ISR*^{GDF15} score or *GDF15* expression in ER or HI, with BH correction. (**D**) Proliferation scores of each tissue split into two groups based on whether the tissue had a higher ISR score in ER or HI from **Figure 2C.** (**E**) Spearman's correlation of *ISR*^{GDF15} scores with proliferation scores. ER = Emergency Room, HI = hospital inpatient.

Figure 1

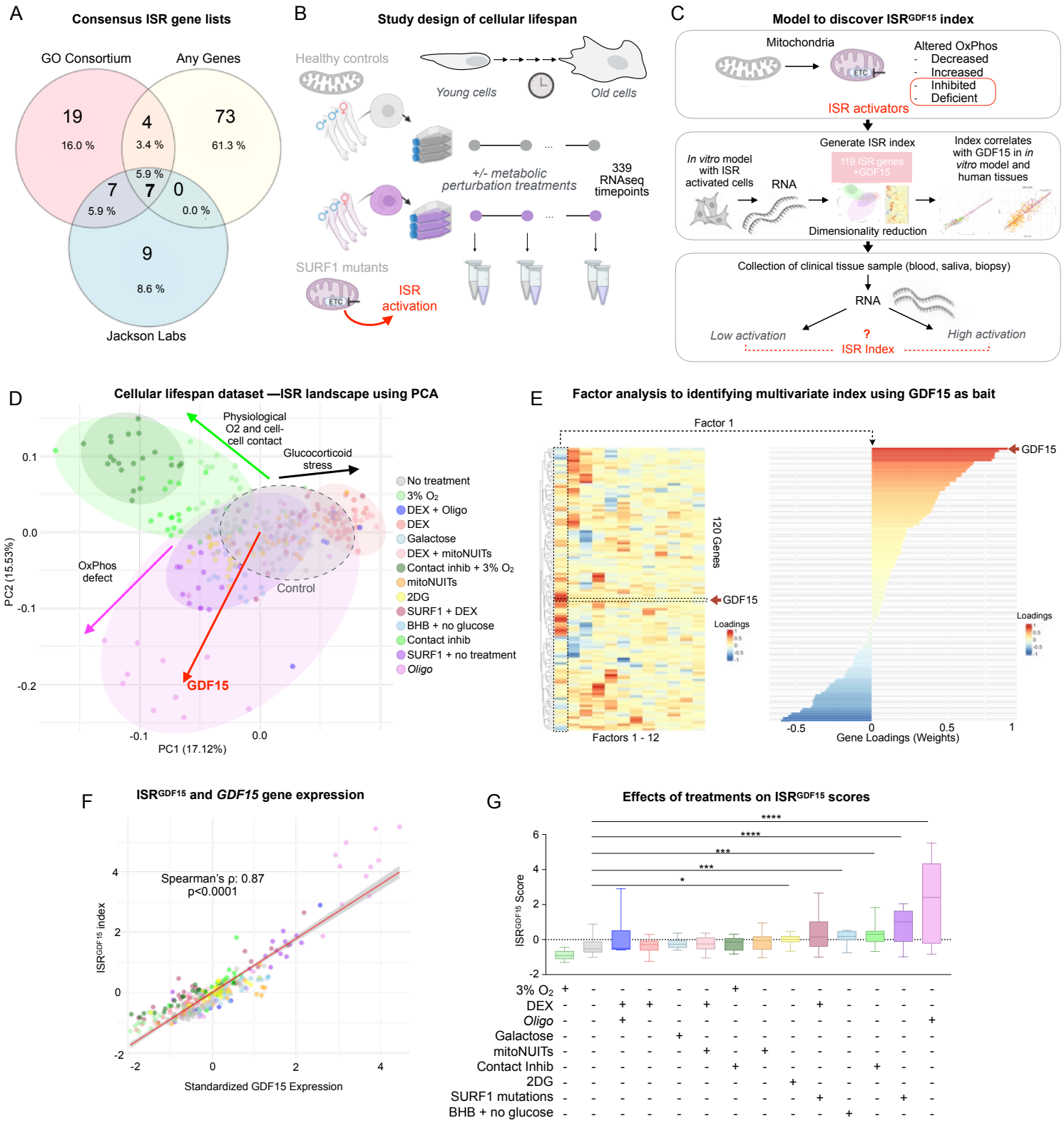

Figure 1. Development of an ISR index using primary human fibroblasts. (**A**) ISR related genes from three reference ISR pathway lists revealing minimal overlap. We use all 119 genes plus *GDF15* (n=120) to compile an unbiased ISR gene list. (**B**) Bulk RNA seq data in primary human fibroblasts from three healthy donors and three individuals with mitochondrial disease (SURF1 gene mutations) were cultured across their replicative lifespans (up to 260 days) and treated with pharmacological and metabolic perturbations, including the OxPhos inhibitor oligomycin (1nM). (**C**) Overview of the analytical strategy to generate an ISR index using *GDF15* as a bait. (**D**) Principal component analysis (PCA) of data from the lifespan study depicted in panel B including 339 samples 120 genes. The red arrow denotes the loading vector of *GDF15*; all other genes shown in **Extended Data Figure 2**. (**E**) Factor analysis revealed one factor where *GDF15* had the strongest positive loading (Factor 1, *left*), yielding weights that reflect the co-regulation of all other genes with *GDF15* (*right*). (**F**) Correlation of Factor 1 with standardized *GDF15* expression. (**G**) Boxplots of ISR^{GDF15} scores for each condition, sorted by ascending median score. P-values from Kruskal-Wallis test and Dunn's test for multiple comparisons. *Oligo,* Oligomycin; DEX = dexamethasone, mitoNUITs = mitochondrial nutrient uptake inhibitors, 2DG = 2-Deoxy-D-glucose, BHB = β-hydroxybutyrate, contact inhib = contact inhibition.

Figure 2

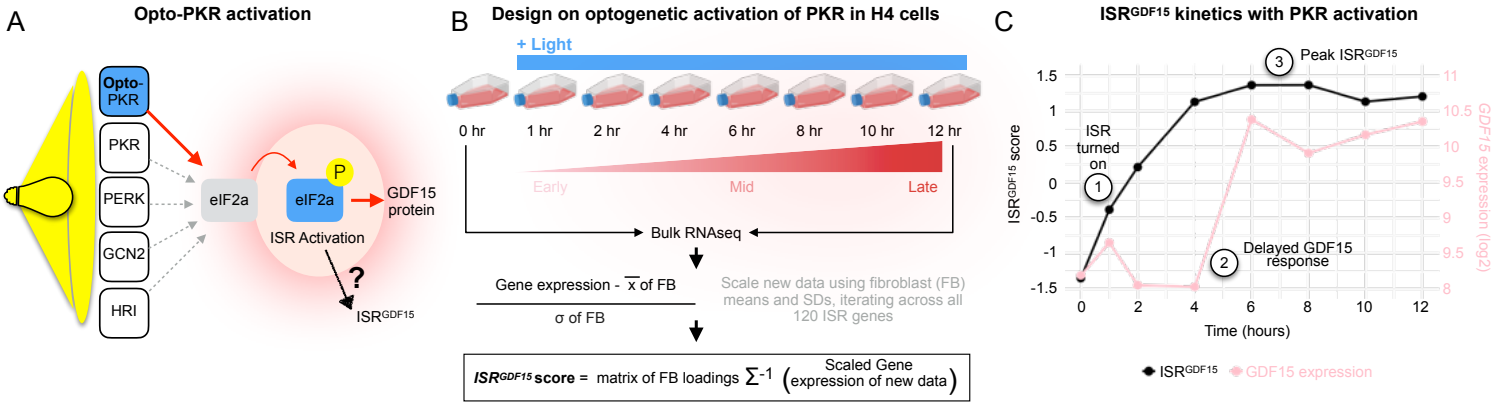

Figure 2. Validation of the ISR^{GDF15} index with time-resolved ISR activation. (**A**) Optogenetic ISR activation strategy targeting an engineered light-sensitive PKR, an ISR kinase, which phosphorylates eIF2alpha to activate the ISR, as per Batjargal et al. (**B**) Experimental and data processing scheme to compute the *ISR^{GDF15}* scores across 8 timepoints spanning 12 hours of continuous PKR activation in H4 cells. (**C**) *ISR^{GDF15}* score and *GDF15* RNA transcript levels for the H4 cells under increasing hours of ISR stimulation.

Figure 3

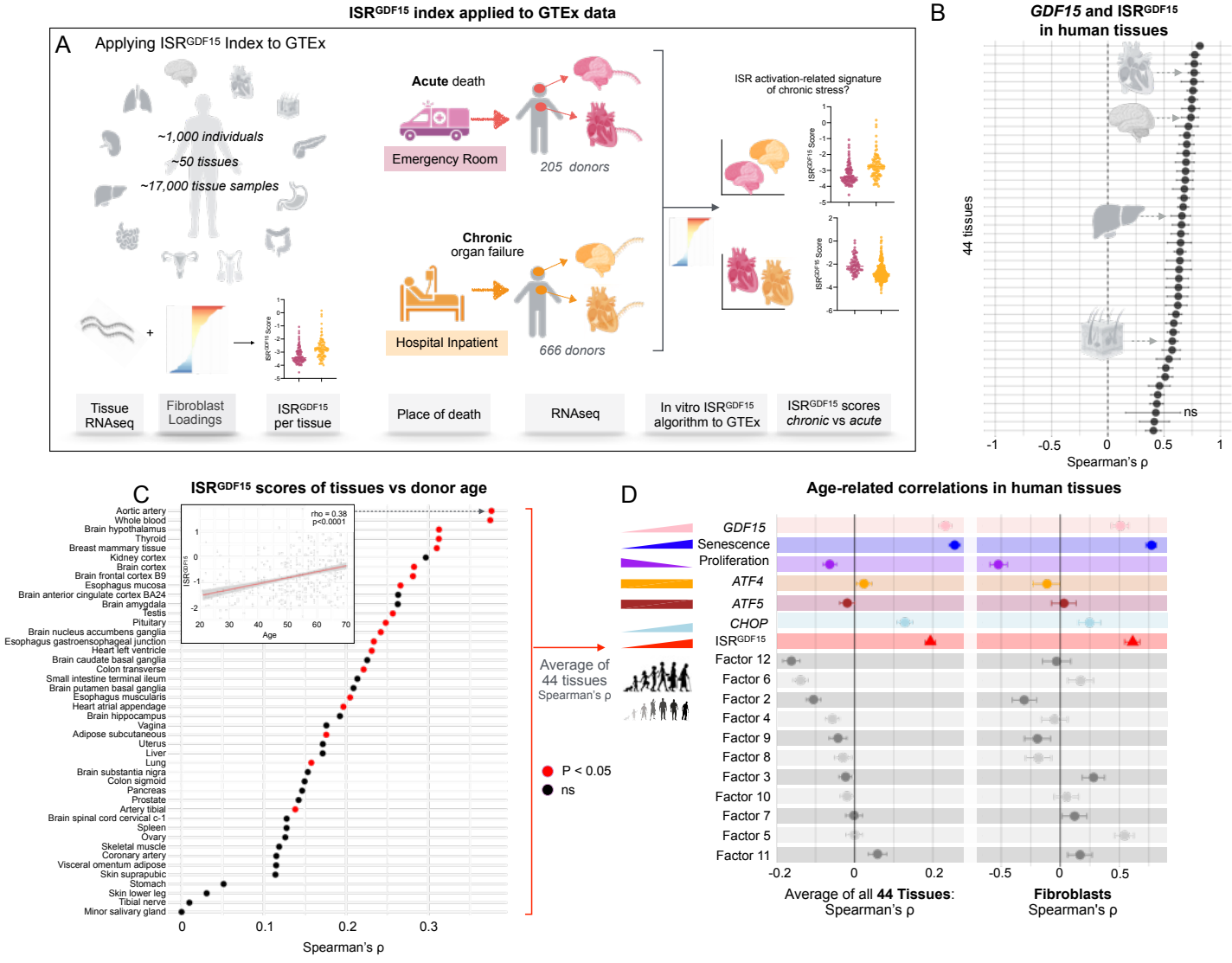

Figure 3. ISR^{GDF15} index applied to human GTEx dataset correlated with age at death. (**A**) Schematic of human GTEx dataset containing a variety of human organ samples, and applying the fibroblast generated index to the human transcriptomic data to get the human *ISR^{GDF15}* scores for each tissue. (**B**) *ISR^{GDF15}* correlations with *GDF15* across all the tissue samples expressing all 120 genes in the *ISR^{GDF15}* index (Spearman's ρ, +/- 95% confidence intervals, Bonferroni corrected for multiple comparisons). (**C**) Spearman's rank correlations of each tissue's *ISR^{GDF15}* score compared to donor age (red points denoting a Bonferroni corrected p<0.05). (**D**) Average Spearman's correlations (+/- SEM) across all 44 tissues comparing the donor age with the chosen gene(s) or *ISR^{GDF15}* score or factor scores (left) and fibroblasts' age correlated with the chosen genes or *ISR^{GDF15}* score or factor score (+/- 95% confidence interval) (right). *ISR^{GDF15}* average tissue correlation denoted with a red triangle. Wilcoxon signed-rank test used compared against 0.

Figure 4

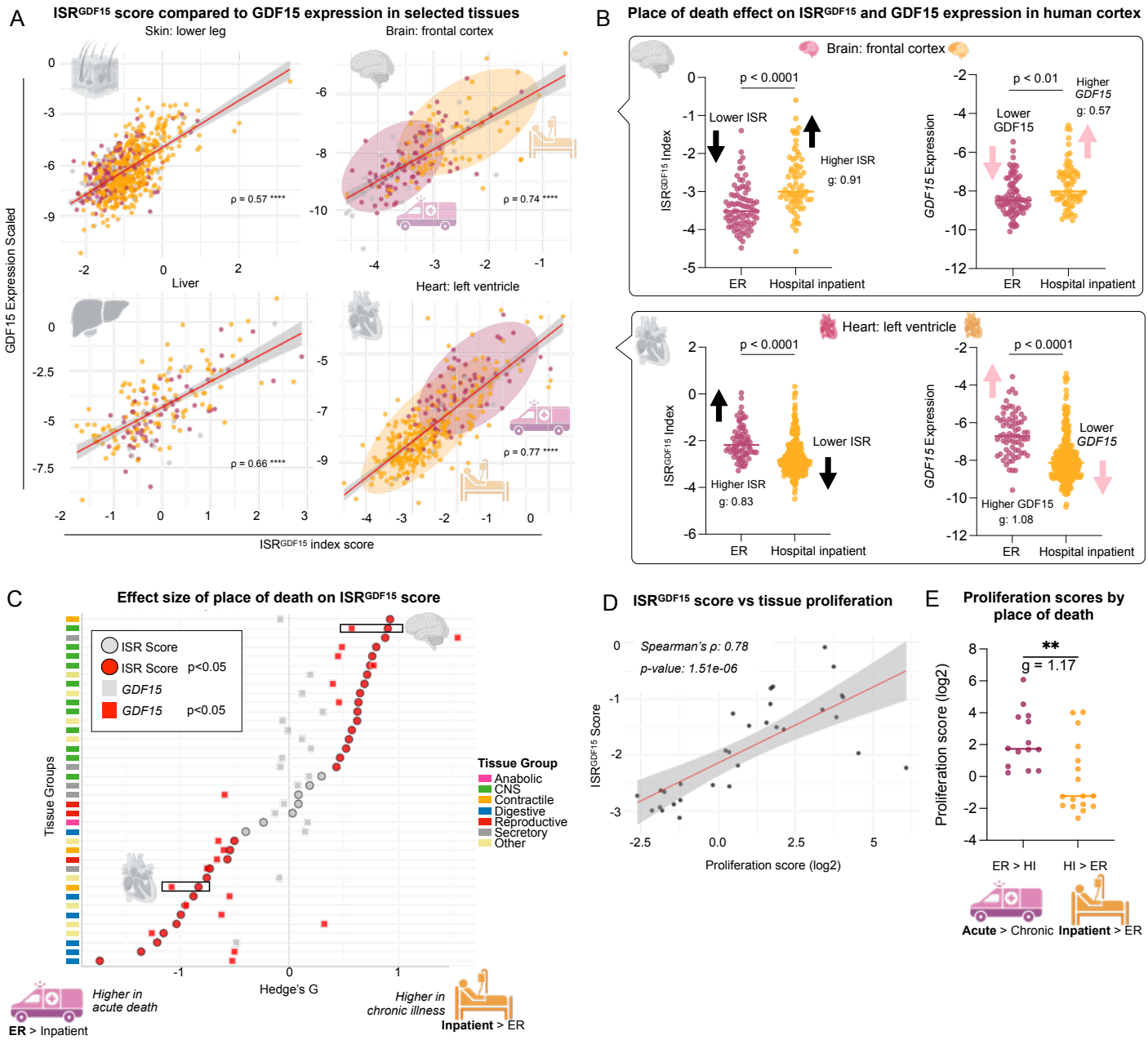

Figure 4. *ISR*^{GDF15} index applied to human GTEx dataset. (**A**) Select tissue correlations of *ISR*^{GDF15} and *GDF15* expression, Bonferroni corrected. (**B**) *ISR*^{GDF15} or *GDF15* expression for each place of death, in brain frontal cortex or heart left ventricle; significance determined via Wilcoxon rank-sum test. (**C**) Hedge's g effect sizes comparing each tissue's *ISR*^{GDF15} activation score for each place of death, or *GDF15* expression comparing each place of death—Hedge's g values of hospital inpatient scores being greater than ER seen on the right, ER greater than hospital inpatient towards the left. Circles denote *ISR*^{GDF15} score, squares *GDF15* expression, red as significant, gray non-significant, with BH correction for multiple comparisons. The grey brain and heart indicate the *ISR*^{GDF15} score and *GDF15* expression of the brain frontal cortex and the heart left ventricle comparisons from **B**. See methods for specific tissues within each tissue grouping. Wilcoxon rank-sum test was used to compare either the *ISR*^{GDF15} score or *GDF15* expression in ER or HI, with BH correction. (**D**) Proliferation scores of each tissue split into two groups based on whether the tissue had a higher ISR score in ER or HI from **Figure 2C**. (**E**) Spearman's correlation of *ISR*^{GDF15} scores with proliferation scores. ER = Emergency Room, HI = hospital inpatient.

Extended Data Figure 1

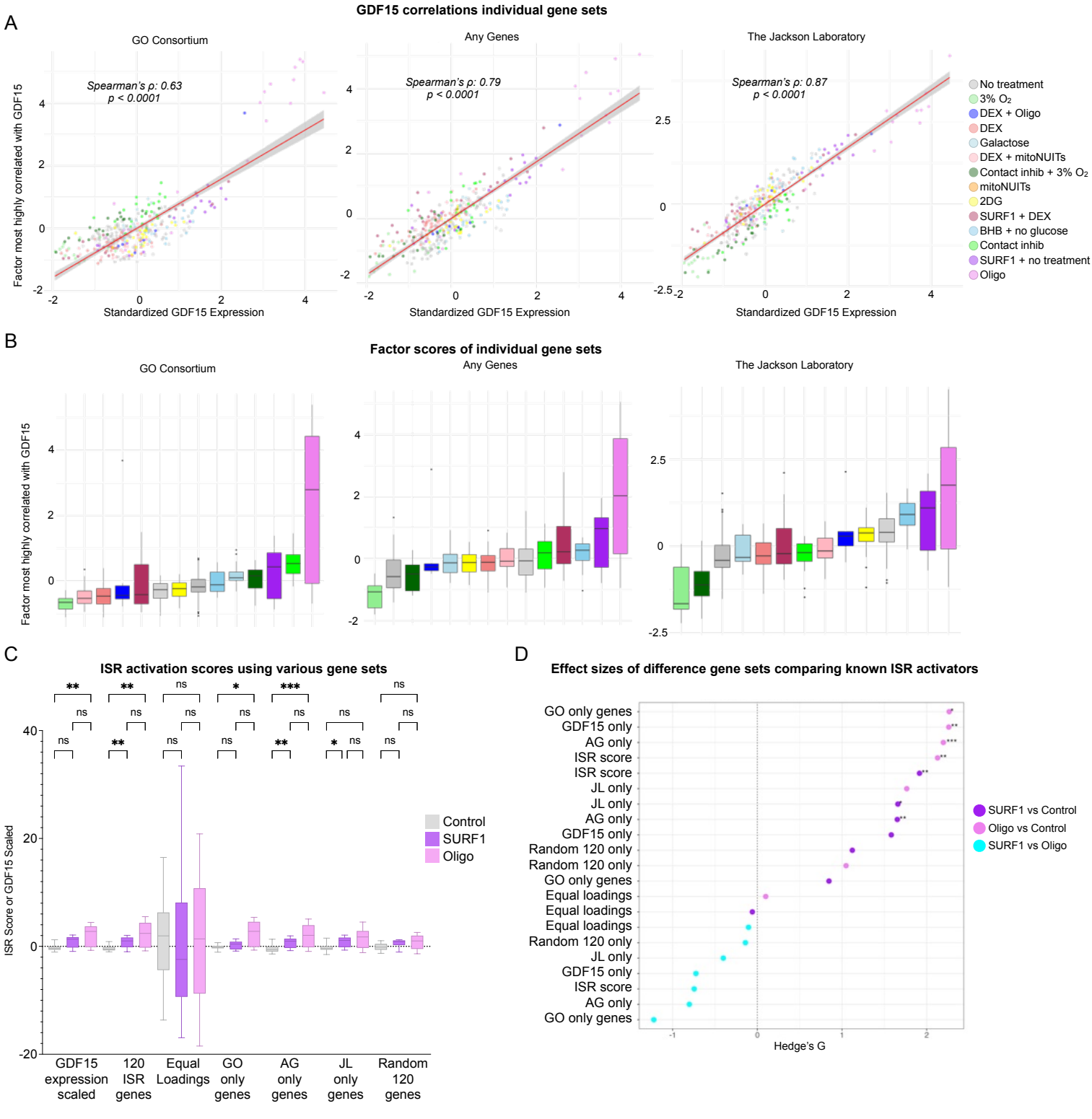

Extended Data Figure 1. Sensitivity analysis for various ISR gene lists. (**A**) Factor analysis performed on individual gene sets (GO Consortium which contained 37 genes, Any Genes which had 84 genes, and Jackson Laboratory which had 23 genes), as well as equal loadings for all the 120 genes (not shown), and the average of 20 different sets of 119 randomly chosen genes plus GDF15 (not shown). The factor that was most correlated with *GDF15* was chosen for further sensitivity analyses. (**B**) The index scores of the chosen factors from individual gene sets depicted in **A**. (**C**) Comparison of the index scores of only control, SURF1 mutant, or Oligo treated cells for each gene set, including equal loadings of the 120 ISR genes; Kruskal-Wallis test performed with Dunn's test for multiple testing. (**D**) The effect sizes of each treatments comparisons (Hedge's g) from panel **C**. GO = GO Consortium, AG = Any Genes, JL = Jackson Laboratory

Extended Data Figure 2

A

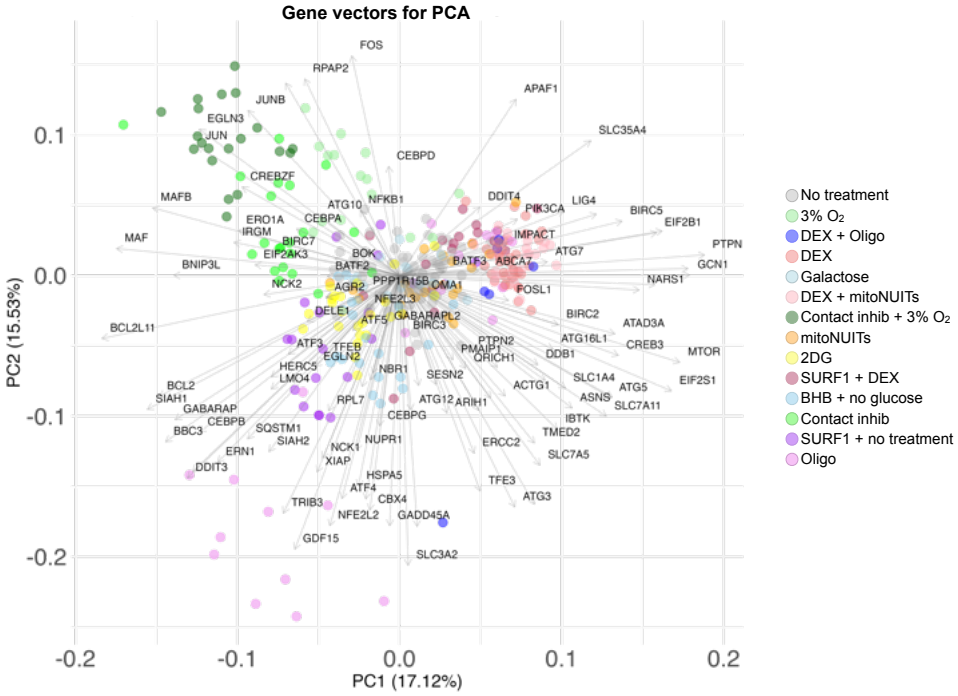

B

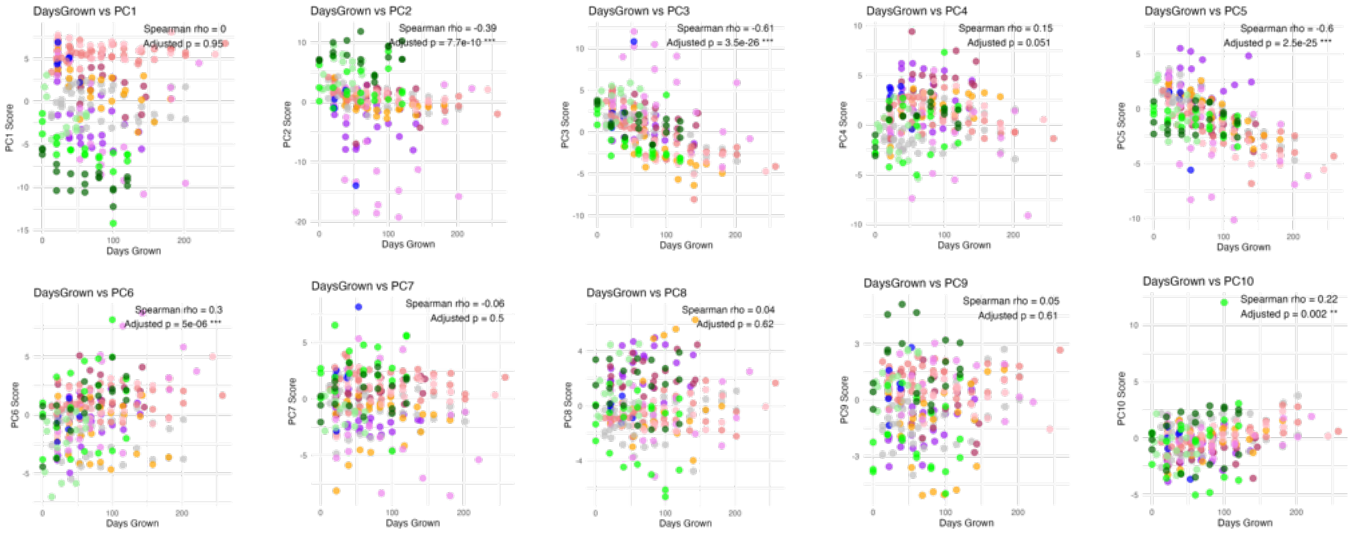

C

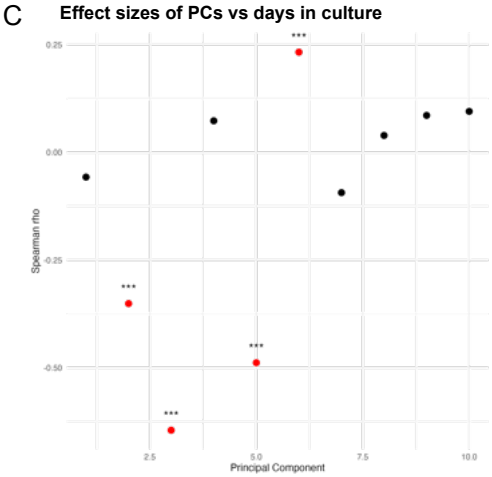

Extended Data Figure 2. Principal component gene vectors and comparisons with age. (**A**) Biplot with gene vector loadings of PC1 and PC2. (**B**) First 10 PC components vs fibroblast time in culture (days). (**C**) Effect sizes (Spearman's rank correlations) of PCs vs time in culture (days).

Extended Data Figure 3

A

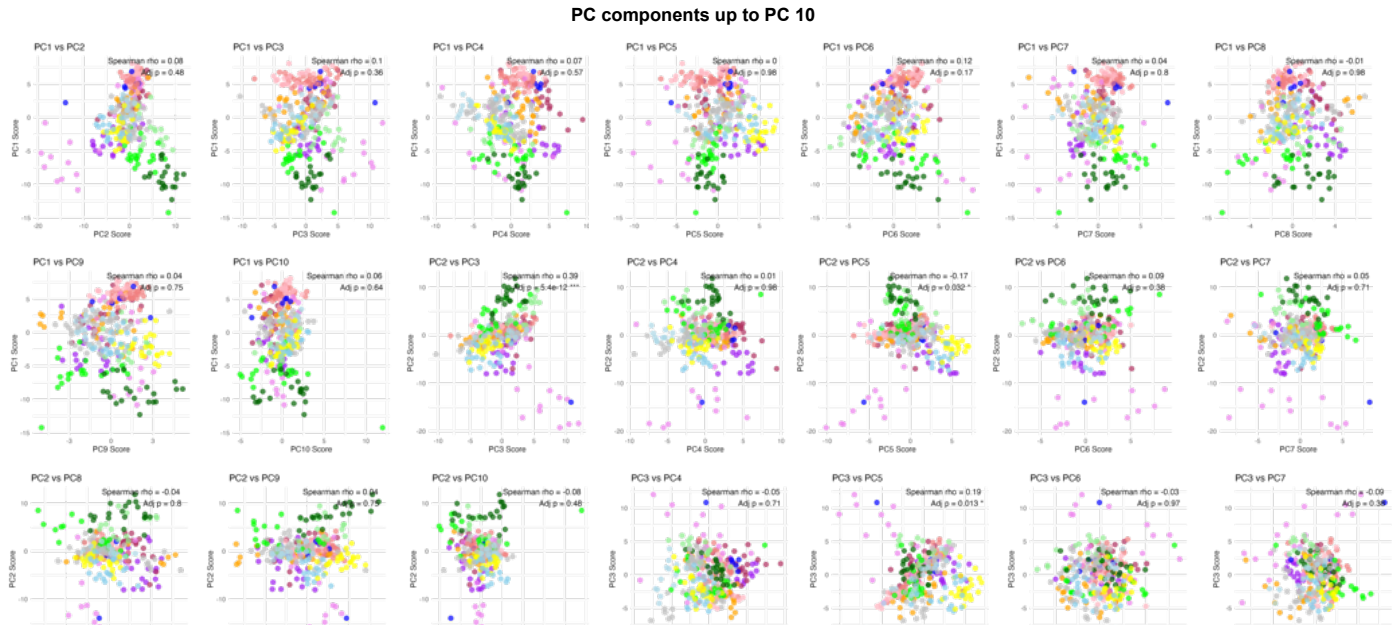

Extended Data Figure 4

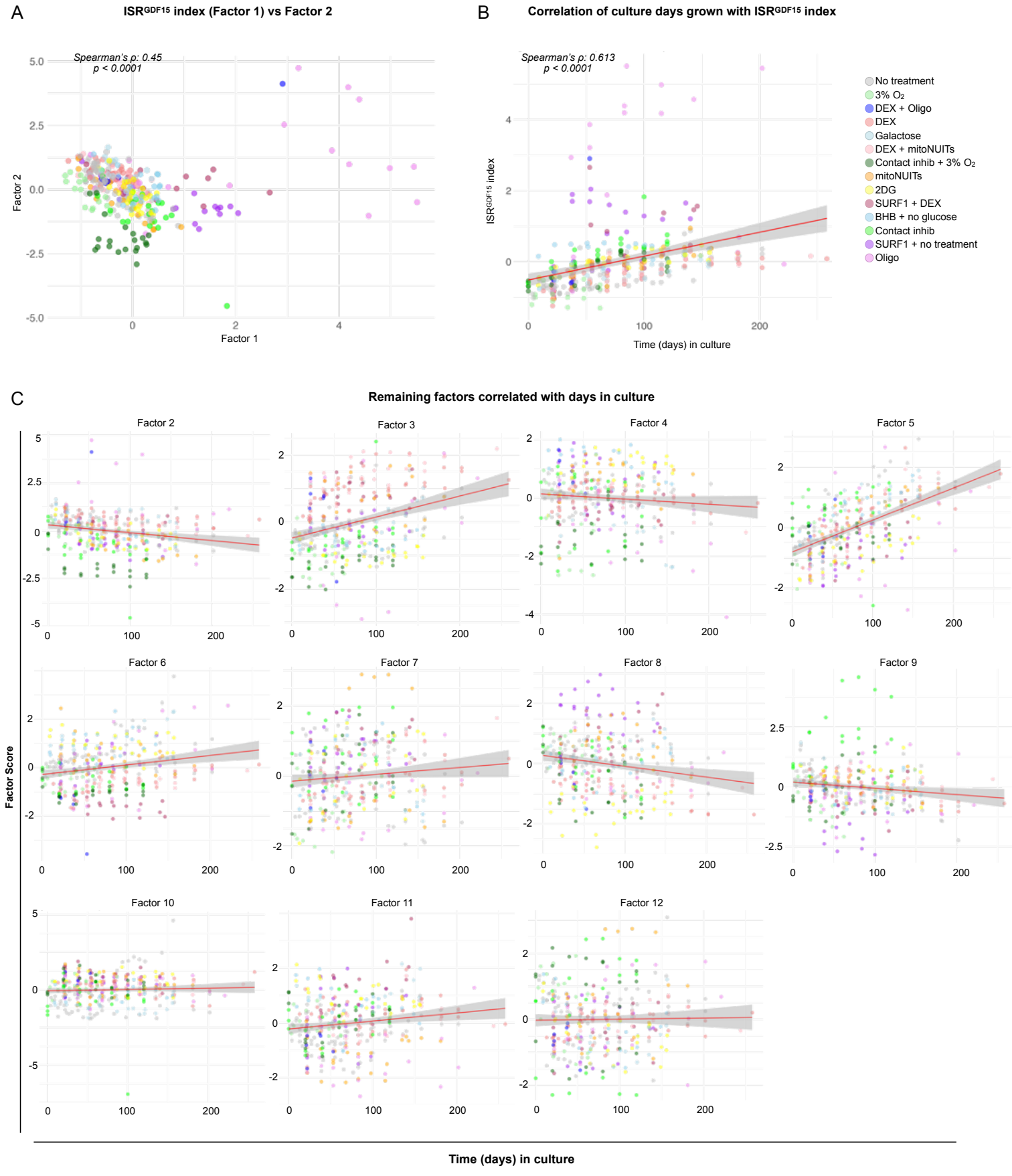

Extended Data Figure 4. Factor analysis comparisons with age. (**A**) Plot of first two factors from the factor analysis. (**B**) Correlation of each fibroblast sample vs time (in days) of culture. (**C**) Remaining 11 factors scores vs time in culture.

Extended Data Figure 5

A

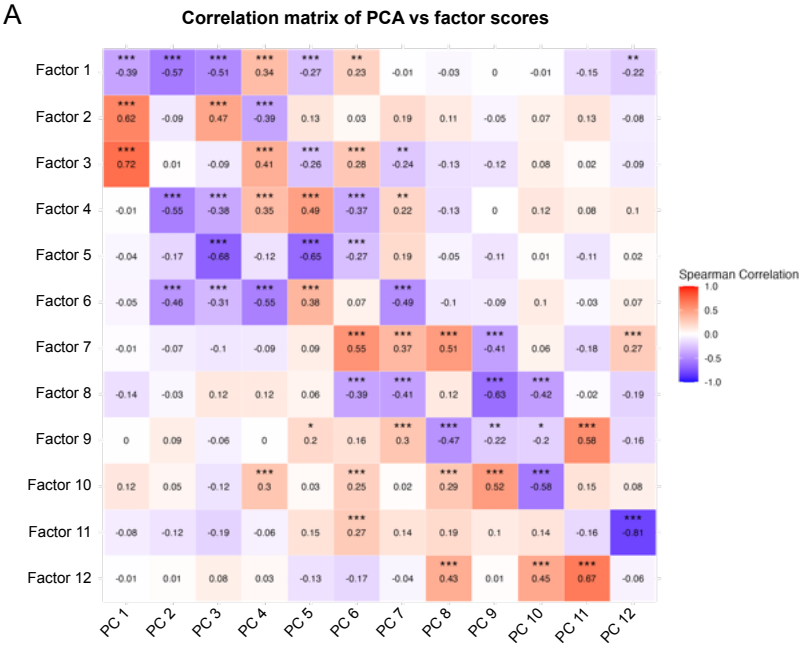

B

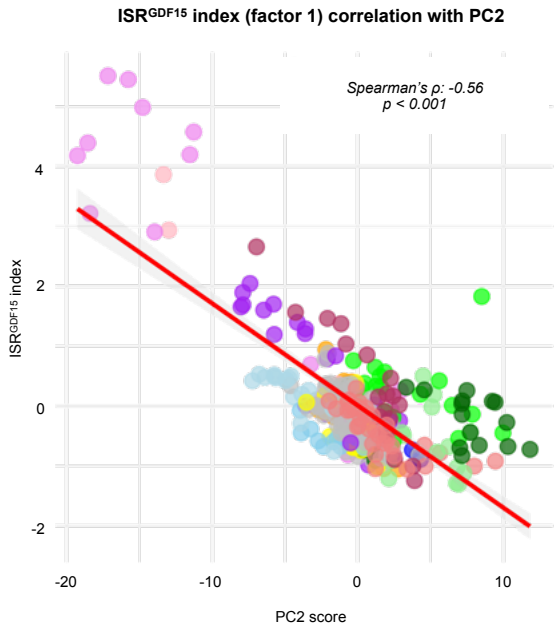

C

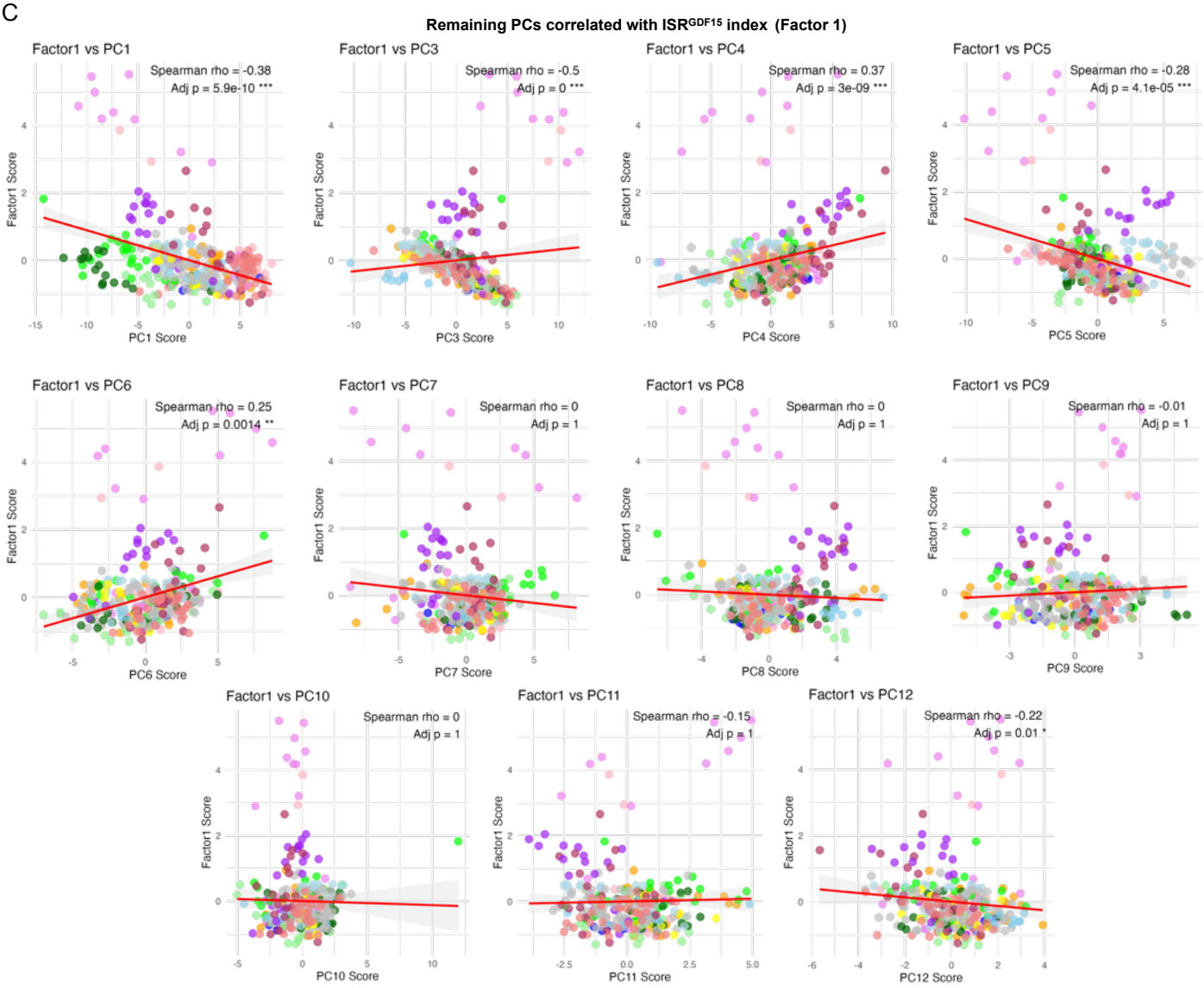

Extended Data Figure 5. Correlations of factor scores and principal components. (**A**) Correlation matrix of Spearman's rank correlations of the factor scores vs the first 12 principal components from the PCA. (**B**) Spearman's correlation of *ISR*^{GDF15} index (Factor 1) vs PC2 score. (**C**) Spearman's correlations of *ISR*^{GDF15} vs remaining principal components up to 12.

Extended Data Figure 6

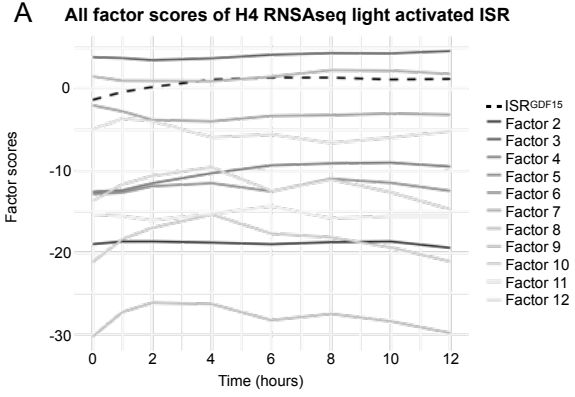

Extended Data Figure 6. All factors applied to opto-PKR H4 cells (**A**) Each factor score for the H4 cells, containing the ISR sensor kinase PKR engineered to be activate in response to light (opto-PKR), stimulated with 0–12 hours of light.

Extended Data Figure 7

A

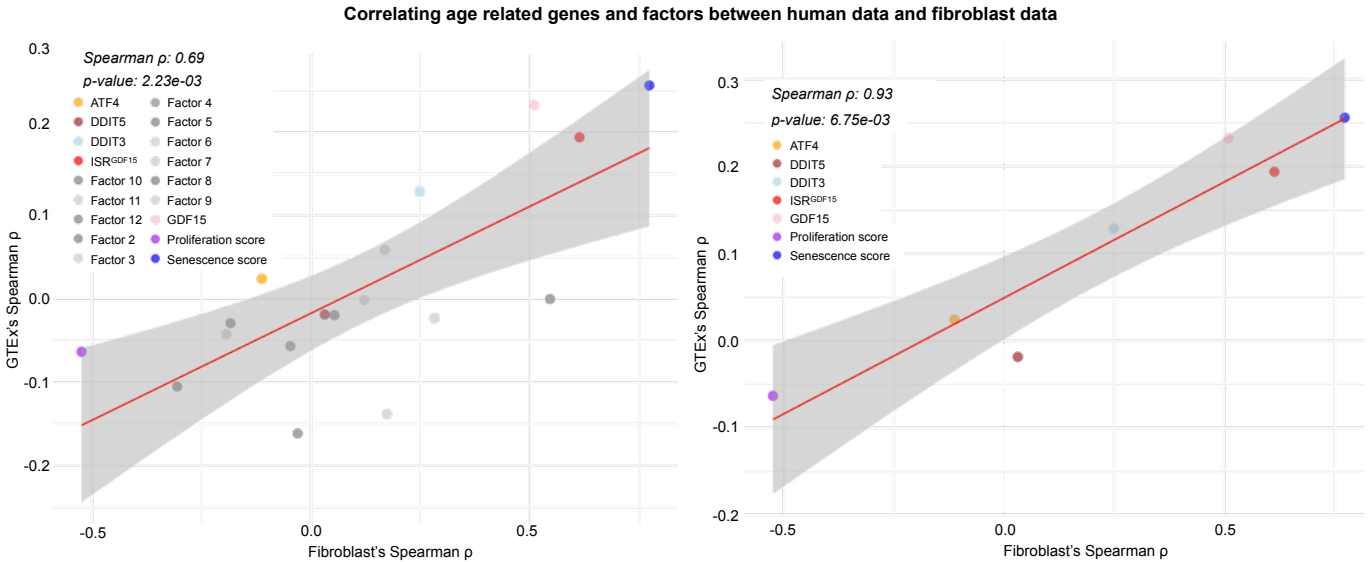

Extended Data Figure 7. Correlations between human and fibroblast age associations with genes and factors (**A**) Spearman's correlations of the average Spearman's ρs of all tissues comparing donor age to chosen genes, *ISR*^{GDF15} score, or other 11 factor scores (left). The panel on the right shows the same plot without the 11 non-*ISR*^{GDF15} factors.

Extended Data Figure 8

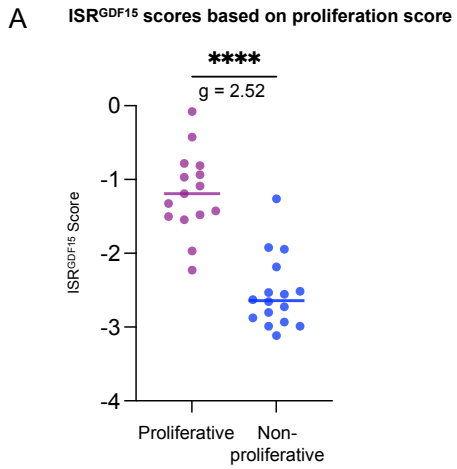

Extended Data Figure 8. Human tissues' *ISR*^{GDF15} scores split based on proliferation status (**A**) *ISR*^{GDF15} score of each tissue split into two groups based on their proliferation score, using the median proliferation score to split the groups. Only the 31 tissues that were significant in *Figure 4C* are included, p-value determined by Mann-Whitney test.

GO Consortium	Any Genes	Jackson Labs
ARIH1	ACTG1	Abca7
ATAD3A	AKT1	Agr2
ATF4	APAF1	Agr2
BATF	ASNS	Atf4
BATF2	ATF3	Bok
BATF3	ATF4	Dele1
CEBPA	ATF5	Eif2ak1
CEBPB	ATF6	Eif2ak3
CEBPD	ATG10	Eif2ak4
CEBPE	ATG12	Eif2s1
CEBPG	ATG16L1	Gcn1
CREB3	ATG3	Impact
CREBZF	ATG5	Igtp
DDIT3	ATG7	Map3k20
DELE1	BBC3	Nck1
EIF2AK1	BCL2	Nck2
EIF2AK3	BCL2L11	Nfe2l2
EIF2AK4	BECN1	Oma1
EIF2S1	BIRC2	Ptpn1
FOS	BIRC3	Ptpn2
FOSL1	BIRC5	Qrich1
GCN1	BIRC7	Rpap2
HERC5	BNIP3L	Tmed2
IMPACT	CBX4	Tmem33
JUN	CEBPB	
JUNB	CEBPG	
LIG4	DDB1	
MAF	DDB2	
MAFB	DDIT3	
MAP3K20	DDIT4	
NFE2	EGLN2	
NFE2L2	EGLN3	
NFE2L3	EIF2AK1	
OMA1	EIF2AK2	
QRICH1	EIF2AK3	
RPAP2	EIF2AK4	
TMED2	EIF2B1	
	EIF2S1	
	EIF2S3	
	ERCC1	
	ERCC2	
	ERCC3	
	ERN 1	
	ERO1A	

FOS
GABARAP
GABARAPL2
GADD45A
GCN1
HSPA5
IBTK
LMO4
MAP1LC3A
MTOR
NAIP
NARS
NBR1
NFE2L2
NFKB1
NUPR1
PIK3CA
PMAIP1
PPP1CA
PPP1R15A
PPP1R15B
RPL7
SESN2
SIAH1
SIAH2
SLC1A4
SLC35A4
SLC38A2
SLC3A2
SLC7A11
SLC7A5
SQSTM1
TFE3
TFEB
TNFRSF10B
TRIB3
TXNIP
WARS
XBP1
XIAP

	Factor1	Factor2	Factor3	Factor4	Factor5
QRICH1	-0.029	0.496	-0.167	0.04	0.042
SLC1A4	0.217	0.156	0.53	0.376	-0.097
ABCA7	0.097	-0.108	0.578	-0.112	0.27
ATAD3A	-0.117	0.692	0.268	0.043	-0.486
SLC35A4	-0.554	0.091	0.382	0.108	0.201
AGR2	0.126	0.003	-0.189	-0.108	-0.01
GCN1	-0.299	0.595	0.543	0.054	-0.226
SLC3A2	0.669	0.284	0.044	0.535	-0.04
DELE1	0.12	-0.079	-0.336	0.192	0.033
SLC7A11	0.045	0.175	0.532	0.684	0.088
ATF4	0.437	0.153	-0.279	0.677	-0.194
HERC5	0.425	-0.321	-0.019	0.11	-0.201
SLC7A5	0.224	0.297	0.313	0.475	0.185
ARIH1	0.321	-0.013	0.331	0.138	0.328
NARS1	-0.39	0.142	0.552	0.521	0.279
RPAP2	-0.285	-0.796	0.142	-0.035	-0.131
APAF1	-0.589	0.03	0.067	-0.094	-0.325
BATF2	-0.156	-0.061	-0.308	0.121	0.152
BBC3	0.678	-0.255	-0.327	0.158	0.17
EIF2S1	-0.09	0.813	0.309	0.13	0.048
BCL2	0.519	-0.134	-0.515	0.03	-0.117
BATF3	-0.121	0.132	0.029	0.073	-0.501
BIRC2	-0.166	0.28	0.168	0.061	0.311
BOK	-0.042	-0.028	-0.283	0.038	-0.019
OMA1	0.07	0.001	0.121	-0.009	0.128
BIRC3	0.237	0.051	0.036	-0.025	-0.035
EIF2AK1	-0.098	0.51	0.011	0.113	0.272
BIRC5	-0.402	0.587	0.185	-0.071	-0.549
IMPACT	-0.474	-0.024	0.069	0.426	0.292
ATG3	0.392	0.779	0.049	0.102	-0.099
NFE2	-0.01	0	0.062	-0.003	-0.052
ATG5	-0.026	0.528	0.29	0.303	0.207
NFE2L3	0.171	0.07	-0.098	0.005	-0.574
ATG7	-0.38	0.462	-0.011	0.16	-0.21
CREBZF	0.059	-0.323	-0.316	-0.154	-0.168
GABARAP	0.405	0.025	-0.684	-0.058	0.342
EIF2AK4	-0.39	0.548	0.464	0.041	0.132
GABARAPL2	0.081	-0.015	-0.007	-0.084	0.887
CEBPE	0.089	-0.114	-0.037	-0.204	-0.215
NBR1	0.335	0.202	-0.069	-0.147	0.635
EIF2AK3	0.122	-0.436	-0.131	0.019	0.188
FOSL1	-0.18	0.355	0.079	-0.083	-0.388
SQSTM1	0.368	0.02	-0.351	0.071	0.213
FOS	-0.534	-0.453	-0.043	0.056	0.014
ASNS	0.086	0.278	0.329	0.728	0.125

CREB3	0.196	0.345	0.727	-0.025	-0.016
BECN1	0.054	0.583	0.415	-0.025	0.383
NFE2L2	0.594	0.071	-0.146	0.563	0.169
EIF2AK2	0.029	0.054	-0.208	0.183	0.154
JUN	-0.025	-0.582	-0.248	-0.184	0.312
MAP3K20	0.106	-0.088	-0.162	-0.024	-0.119
BATF	-0.012	-0.005	0.307	-0.007	0.005
MAF	0.066	-0.331	-0.75	-0.046	0.078
CEBPD	-0.118	-0.045	-0.053	0	0.137
MAP1LC3A	0.219	0.327	0.252	-0.062	0.469
LIG4	-0.338	-0.187	0.56	0.235	0.461
SLC38A2	-0.187	0.099	0.518	0.031	-0.08
DDB1	-0.17	0.446	0.117	0.028	0.23
IRGM	0.17	-0.485	-0.139	-0.091	-0.026
CEBPG	0.231	-0.082	-0.08	0.881	-0.142
DDB2	0.419	-0.142	0.136	0.018	0.477
CEBPB	0.634	0.197	-0.463	-0.165	0.08
DDIT4	-0.06	-0.115	0.357	0.144	0.052
JUNB	-0.277	-0.437	-0.286	-0.066	0.061
ATF6	0.016	0.165	0.367	0.367	0.461
TMED2	0.01	0.505	-0.062	0.432	0.107
HSPA5	0.488	0.13	-0.106	0.419	-0.414
CEBPA	0.09	-0.162	-0.067	-0.179	-0.028
NCK1	0.451	0.252	-0.329	0.186	0.226
DDIT3	0.844	-0.078	-0.303	0.042	-0.019
PIK3CA	-0.375	-0.046	0.172	0.163	0.589
MAFB	0.111	-0.323	-0.545	-0.219	-0.079
AKT1	-0.127	0.655	0.42	-0.116	-0.092
IBTK	-0.027	0.398	0.097	0.594	-0.055
NCK2	0.056	-0.103	-0.422	0.096	-0.019
MTOR	-0.112	0.503	0.624	0.269	0.103
ACTG1	0.159	0.654	-0.026	-0.046	-0.204
EIF2B1	-0.391	0.515	0.334	0.027	0.125
EIF2S3	0.069	0.516	-0.12	0.253	0.067
PPP1CA	-0.602	0.628	0.202	0.125	-0.272
RPL7	0.166	0.395	-0.61	0.226	0.209
PTPN1	-0.239	0.353	0.808	-0.048	0.19
SESN2	0.131	-0.259	0.259	0.771	0.03
WARS1	-0.126	0.121	0.018	0.896	0.1
BCL2L11	0.399	-0.36	-0.618	0.103	-0.025
PTPN2	0.199	0.449	0.014	-0.043	-0.331
ERN1	0.815	-0.313	-0.034	0.175	-0.003
ERO1A	-0.058	-0.183	-0.559	-0.247	0.101
PPP1R15A	0.819	0.114	-0.389	-0.087	-0.065
PPP1R15B	0.147	-0.132	0.108	0.33	-0.198
TRIB3	0.623	-0.073	-0.172	0.696	-0.045

XBP1	0.485	0.158	-0.145	0.706	-0.283
TMEM33	0.412	0.579	0.249	0.227	-0.022
ERCC1	0.083	0.331	-0.317	-0.043	-0.175
ERCC2	0.312	0.634	-0.047	0.006	-0.162
ERCC3	0.097	0.265	-0.114	0.161	0.277
GADD45A	0.814	0.247	0.184	0.058	0.045
BNIP3L	0.154	-0.173	-0.651	-0.233	0.424
ATF3	0.351	-0.133	-0.061	-0.001	-0.155
ATF5	0.195	-0.053	0.035	0.058	-0.202
CBX4	0.797	0.217	0.144	0.156	-0.032
EGLN2	0.277	0.283	-0.277	-0.115	-0.067
EGLN3	-0.026	-0.528	-0.323	-0.34	-0.01
LMO4	0.228	-0.063	-0.375	0.375	-0.008
NFKB1	-0.31	0.153	-0.352	0.006	-0.054
TFE3	0.439	0.67	0.01	0.037	0.013
TFEB	0.562	0.081	0.027	-0.226	0.032
TXNIP	-0.249	-0.013	0.192	0.185	0.423
BIRC7	0.204	-0.251	-0.103	-0.177	-0.234
NAIP	-0.461	-0.715	-0.183	0.16	-0.132
NUPR1	0.518	0.15	-0.003	0.254	0.438
PMAIP1	0.08	0.087	0.092	0.356	-0.47
SIAH1	0.45	-0.093	-0.71	0.203	-0.147
SIAH2	0.651	-0.042	-0.224	0.354	-0.037
TNFRSF10B	0.598	0.058	0.259	0.424	0.28
XIAP	0.56	0.015	-0.014	0.076	0.066
ATG10	0.022	-0.509	0.1	0.122	-0.084
ATG12	0.196	0.198	-0.074	0.053	0.664
ATG16L1	0.2	0.123	0.592	0.098	0.023
GDF15	0.902	0.057	0.026	0.231	0.12

Factor6	Factor7	Factor8	Factor9	Factor10	Factor11
0.386	-0.228	-0.058	0.39	0.161	-0.056
-0.103	0.286	-0.153	-0.123	0.327	0.132
0.041	0.31	-0.009	0.188	-0.089	-0.036
-0.028	-0.008	0.006	-0.088	-0.178	0.088
-0.189	0.092	-0.222	0.205	0.028	0.413
0.057	-0.072	-0.03	-0.06	-0.043	0.084
-0.063	0.066	0.005	0.047	-0.071	0.014
0.206	-0.17	-0.178	-0.077	0.01	0.023
-0.134	0.392	0.094	-0.248	0.145	0.258
0.174	-0.176	0.019	-0.024	0.174	-0.004
-0.045	-0.089	0.243	-0.215	-0.001	-0.078
0.446	-0.048	-0.041	0.196	0.1	0.003
0.27	-0.443	-0.041	-0.216	-0.051	-0.052
0.445	-0.044	0.208	0.09	0.319	-0.082
0.198	0.097	0.078	0.003	-0.072	0.119
-0.022	0.052	0.023	0.07	0.032	-0.141
-0.239	-0.327	0.139	-0.14	0.207	-0.264
0.413	-0.017	-0.216	0.327	-0.281	-0.005
0.066	-0.121	0.132	0.06	-0.298	-0.118
0.098	-0.051	-0.125	0.043	0.199	-0.132
0.155	-0.038	-0.047	0.148	-0.21	0.141
0.097	0.045	0.162	-0.025	-0.047	-0.15
0.386	-0.1	-0.051	-0.105	0.482	0.06
-0.208	-0.596	0.177	-0.444	-0.112	-0.008
0.018	0.746	-0.147	0.062	0.144	0.078
0.015	0.138	-0.447	0.004	0.215	0.176
0.374	0.384	-0.059	-0.081	0.344	0.113
-0.123	0.003	-0.235	-0.007	0.035	-0.006
0.137	-0.009	0.476	-0.164	0.006	-0.016
0.234	0.03	-0.143	0.072	-0.083	-0.046
0.052	0.052	-0.026	0.078	-0.035	-0.013
0.124	-0.085	-0.082	0.111	0.177	-0.102
-0.043	-0.057	0.185	0.057	0.127	-0.3
-0.076	0.01	-0.003	-0.008	-0.325	-0.201
-0.466	-0.014	0.231	-0.012	0.037	-0.23
0.392	0.046	0.075	-0.053	-0.142	0.058
0.018	-0.249	0.191	-0.1	-0.064	-0.135
0.2	0.033	-0.012	-0.066	-0.014	-0.029
0.168	0.009	-0.041	0.008	-0.049	0.017
-0.135	0.04	0.188	0.068	-0.03	-0.459
0.272	0.282	-0.07	0.182	0.155	0.483
0.507	-0.076	0.127	-0.031	-0.01	0.263
0.642	0.161	0.059	0.045	-0.411	0.086
-0.279	0.104	0.298	0.304	-0.053	0.324
-0.34	-0.199	-0.063	-0.034	0.088	-0.173

-0.147	-0.149	0.11	-0.181	-0.056	-0.103
0.182	-0.086	0.055	-0.074	-0.182	-0.31
0.187	0.036	0.05	0.127	0.218	0.013
0.619	0.029	-0.034	0.117	0.095	-0.008
-0.269	0.094	0.132	0.149	-0.165	0.171
0.044	-0.179	0.608	-0.086	0.173	-0.076
0.06	0.028	-0.184	0.012	-0.009	0.048
0.112	-0.122	-0.084	0.249	-0.305	0.029
-0.867	0.013	-0.039	0.158	-0.018	-0.017
-0.257	-0.098	0.086	-0.331	-0.095	-0.255
0.121	0.03	-0.048	0.125	0.189	0.152
-0.365	0.221	0.089	-0.02	0.511	-0.057
0.583	0.225	0.358	-0.122	-0.121	-0.057
0.095	-0.184	-0.034	-0.003	-0.013	-0.039
-0.147	0.021	0.001	0.017	0.057	0.021
0.085	-0.145	-0.024	-0.126	-0.014	0.007
-0.052	0.054	0.099	0.217	-0.348	-0.005
-0.683	0.065	0.024	-0.093	0.025	0.054
-0.224	0.104	0.276	0.355	-0.068	0.444
0.032	0.031	-0.118	0.003	0.278	0.474
0.396	0.141	-0.29	-0.09	0.357	0.155
0.311	0.095	-0.057	-0.185	0.083	0.266
-0.021	0.08	0.051	0.623	-0.063	0.018
0.152	0.128	-0.286	0.271	0.122	0.09
-0.025	0.114	-0.021	-0.089	-0.141	-0.036
0.039	0.117	0.007	-0.035	0.357	0.129
-0.095	0.105	-0.026	0.378	-0.039	0.336
-0.358	-0.184	-0.103	-0.052	0.076	0.046
0.194	0.048	0.188	-0.25	0.236	0.026
0.054	-0.25	0.108	-0.068	-0.079	0.187
0.107	0.019	0.122	-0.008	-0.037	0.144
-0.175	-0.083	0.347	-0.469	-0.072	-0.059
-0.31	-0.102	-0.044	-0.059	0.125	-0.023
0.034	0.643	-0.107	-0.079	-0.02	-0.009
0.109	-0.039	-0.069	0.027	-0.127	0.053
-0.155	0.04	0.202	-0.103	-0.015	-0.17
-0.023	-0.041	0.004	0.002	0.155	0.026
0.136	0.084	0.134	0.084	-0.168	0.027
0.153	0.084	-0.173	0.033	-0.119	0.023
0.071	-0.022	0.063	0.332	-0.168	-0.067
-0.26	0.205	-0.046	0.051	0.107	-0.052
0.05	0.185	0.025	-0.058	0.05	-0.064
0.24	0.046	-0.156	-0.251	0.17	0.396
-0.064	-0.081	0.067	0.137	-0.123	-0.042
-0.333	-0.087	0.49	0.461	0.041	0.074
0.012	0.111	-0.008	-0.066	-0.12	0.108

-0.036	0.058	-0.073	0.032	0.139	0.107
0.292	0.158	-0.183	0.071	0.15	0.139
-0.471	0.051	-0.069	-0.002	-0.077	0.05
0.003	-0.033	0.233	-0.47	-0.159	-0.014
0.189	-0.484	0.065	-0.048	0.129	0.09
0.092	0.11	-0.006	-0.073	0.113	0.046
-0.005	-0.067	0.127	-0.021	0.047	0.081
0.156	0.084	0.575	0.036	-0.005	0.17
0.077	0.651	0.207	-0.034	-0.045	0.047
-0.169	-0.045	0.293	-0.095	0.046	0.035
0.001	-0.198	-0.037	0.073	-0.606	-0.084
-0.235	0.004	-0.161	-0.044	0.074	0.037
0.024	0.142	0.315	-0.104	-0.035	-0.103
0.029	0.076	-0.231	0.578	-0.316	-0.011
0.03	-0.05	0.061	-0.089	-0.049	-0.227
-0.398	-0.111	-0.105	0.142	-0.039	-0.281
0.002	-0.075	-0.357	0.23	0.092	-0.026
-0.066	0.082	-0.153	-0.068	-0.081	0.103
0.015	0.085	0.099	0.039	0.139	0.057
-0.239	0.001	-0.086	-0.067	-0.366	0.081
0.205	-0.165	0.129	0.024	0.116	-0.029
0.118	-0.104	0.145	0.134	0.012	-0.112
-0.361	-0.086	0.141	-0.1	0.195	-0.02
0.363	-0.037	0.116	-0.104	0.021	0.03
0.518	0.203	0.116	-0.046	0.058	-0.063
-0.086	-0.356	0.172	-0.037	-0.014	-0.028
0.413	-0.091	-0.132	0.077	0.071	-0.128
-0.054	-0.101	0.009	-0.085	0.033	0.031
0.128	0.082	0.047	-0.042	-0.094	-0.019

Factor12
0.062
-0.013
-0.098
-0.061
-0.008
0.082
0.024
-0.063
-0.135
-0.193
-0.086
-0.127
0.067
0.107
0.024
0.135
0.155
-0.263
-0.193
0.144
-0.209
0.19
0.094
0.183
-0.118
-0.227
0.128
-0.045
-0.15
0.056
-0.281
0.005
-0.165
-0.296
-0.062
0.035
-0.18
0.164
0.093
-0.033
0.108
-0.227
0.032
0.003
0.025

-0.006
-0.04
0.012
-0.128
-0.005
-0.111
0.004
0.136
0.07
0.355
0.091
-0.003
0.006
0.019
-0.057
-0.432
0.047
0.128
0.053
-0.119
0.085
-0.085
-0.14
-0.193
0.051
0.143
-0.055
-0.064
0.077
0.215
-0.085
0.233
-0.024
0.018
0.012
-0.203
0.064
-0.088
0.08
0.075
-0.312
0.203
0.17
0.014
0.071
0.112

0.129
0.018
-0.228
0.202
-0.001
-0.218
0.179
0.086
0.274
-0.012
0.039
0.284
0.346
0.006
0.027
0.08
-0.146
0.182
-0.012
0.098
-0.483
0.146
0.249
-0.204
0.339
0.032
-0.005
0.04
-0.014

Top 10 positive genes

DDIT3
PPP1R15A
ERN 1
GADD45A
CBX4
BBC3
SLC3A2
SIAH2
CEBPB
TRIB3

Known functions of positive genes

Activated by ER stress, plays regulatory role in inflammatory response
Involved in autophagy, role in reversing global protein reduction initiated by ISR
Protein which senses unfolded proteins in the ER
Mediates activation of the p38/JNK pathway via MTK1/MEKK4 kinase
Plays a role in negative regulation of transcription by RNA polmerase II
Pro-apoptotic role
Assists biogenesis and trafficking of functional transporters to the plasma membrane
An E3 kinase involved in uibquitination of proteins, implicated in regulating cellular response to h
Regulates the expression of genes relating to immune and inflammatory responses, and other p
Inhibits activity of DDIT3, and acts as a negative feedback regulator of the ISR

Top 10 negative genes	Known functions of negative genes
PPP1CA	Involved in the regulation of many cellular processes, sucl
APAF1	A cytoplasmic protein that initiates apoptosis
SLC35A4	Plays a role in positive regulation of cellular respiration an
FOS	Associated with apoptosis, implicated in regulation of cell
IMPACT	Regulator of translation, promotes high levels of translatio
NAIP	Inhibits activities of caspase 3, 7, and 9, functions to preve
BIRC5	Promotes proliferation and inhibits apoptosis
EIF2B1	Component of the translation initiation factor 2B complex,
NARS1	Catalyzes attachment of asparagine to tRNA, essential rol
GCN2	Phosphorylates eIF2, resulting in down regulation of prote

h as protein synthesis and cell division

d positive regulation of translation in response to stress
proliferation, differentiation, and transformation
n in response to a variety of stressors
ent apoptosis

regulator of protein synthesis
le in protein synthesis
in synthesis in response to low amino acid availability

Genes	Positive Loadings	Genes	Negative Loadings
GDF15	0.902	NFE2	-0.01
DDIT3	0.844	BATF	-0.012
PPP1R15A	0.819	JUN	-0.025
ERN 1	0.815	ATG5	-0.026
GADD45A	0.814	EGLN3	-0.026
CBX4	0.797	IBTK	-0.027
BBC3	0.678	QRICH1	-0.029
SLC3A2	0.669	BOK	-0.042
SIAH2	0.651	ERO1A	-0.058
CEBPB	0.634	DDIT4	-0.06
TRIB3	0.623	EIF2S1	-0.09
TNFRSF10B	0.598	EIF2AK1	-0.098
NFE2L2	0.594	MTOR	-0.112
TFEB	0.562	ATAD3A	-0.117
XIAP	0.56	CEBPD	-0.118
BCL2	0.519	BATF3	-0.121
NUPR1	0.518	WARS1	-0.126
HSPA5	0.488	AKT1	-0.127
XBP1	0.485	BATF2	-0.156
NCK1	0.451	BIRC2	-0.166
SIAH1	0.45	DDB1	-0.17
TFE3	0.439	FOSL1	-0.18
ATF4	0.437	SLC38A2	-0.187
HERC5	0.425	PTPN1	-0.239
DDB2	0.419	TXNIP	-0.249
TMEM33	0.412	JUNB	-0.277
GABARAP	0.405	RPAP2	-0.285
BCL2L11	0.399	GCN1	-0.299
ATG3	0.392	NFKB1	-0.31
SQSTM1	0.368	LIG4	-0.338
ATF3	0.351	PIK3CA	-0.375
NBR1	0.335	ATG7	-0.38
ARIH1	0.321	NARS1	-0.39
ERCC2	0.312	EIF2AK4	-0.39
EGLN2	0.277	EIF2B1	-0.391
BIRC3	0.237	BIRC5	-0.402
CEBPG	0.231	NAIP	-0.461
LMO4	0.228	IMPACT	-0.474
SLC7A5	0.224	FOS	-0.534
MAP1LC3A	0.219	SLC35A4	-0.554
SLC1A4	0.217	APAF1	-0.589
BIRC7	0.204	PPP1CA	-0.602
ATG16L1	0.2		

PTPN2	0.199
CREB3	0.196
ATG12	0.196
ATF5	0.195
NFE2L3	0.171
IRGM	0.17
RPL7	0.166
ACTG1	0.159
BNIP3L	0.154
PPP1R15B	0.147
SESN2	0.131
AGR2	0.126
EIF2AK3	0.122
DELE1	0.12
MAFB	0.111
MAP3K20	0.106
ABCA7	0.097
ERCC3	0.097
CEBPA	0.09
CEBPE	0.089
ASNS	0.086
ERCC1	0.083
GABARAPL2	0.081
PMAIP1	0.08
OMA1	0.07
EIF2S3	0.069
MAF	0.066
CREBZF	0.059
NCK2	0.056
BECN1	0.054
SLC7A11	0.045
EIF2AK2	0.029
ATG10	0.022
ATF6	0.016
TMED2	0.01